MCDONNELL DOUGLAS RESEARCH LABORATORIES

MCDONNELL DOUGLAS CORPORATION

Report MDC Q1203
Contract No. N60921-79-C-0180

LASER RADAR ANALYSES

J. C. Leader

McDonnell Douglas Research Laboratories
St. Louis, Missouri 63166

30 July 1983
Final Report for Period 15 July 1980 – 30 July 1983

Approved for public release; distribution unlimited

Prepared for:

DEPARTMENT OF THE NAVY
Naval Surface Weapons Center
White Oak, Silver Spring, Maryland 20910

MCDONNELL DOUGLAS RESEARCH LABORATORIES

MCDONNELL DOUGLAS
CORPORATION

UNCLASSIFIED

SECURITY CLASSIFICATION OF THIS PAGE *(When Data Entered)*

REPORT DOCUMENTATION PAGE	READ INSTRUCTIONS BEFORE COMPLETING FORM
1. REPORT NUMBER	2. GOVT ACCESSION NO. AD-A133 295	3. RECIPIENT'S CATALOG NUMBER
4. TITLE *(and Subtitle)* LASER RADAR ANALYSES	5. TYPE OF REPORT & PERIOD COVERED Final Report 15 July 1980 - 15 July 1983
	6. PERFORMING ORG. REPORT NUMBER MDC Q1203
7. AUTHOR(s) J. C. Leader	8. CONTRACT OR GRANT NUMBER(s) N60921-79-C-0180
9. PERFORMING ORGANIZATION NAME AND ADDRESS McDonnell Douglas Research Laboratories McDonnell Douglas Corporation St. Louis, MO 63166	10. PROGRAM ELEMENT, PROJECT, TASK AREA & WORK UNIT NUMBERS 62332N: SF 32-399; SF 32-399-492; 9F78EA
11. CONTROLLING OFFICE NAME AND ADDRESS Naval Surface Weapons Center White Oak, Silver Spring, Maryland 20910 Attn: Code F46	12. REPORT DATE 15 July 1983 13. NUMBER OF PAGES 54
14. MONITORING AGENCY NAME & ADDRESS*(if different from Controlling Office)*	15. SECURITY CLASS *(of this report)* Unclassified 15a. DECLASSIFICATION/DOWNGRADING SCHEDULE

16. DISTRIBUTION STATEMENT *(of this Report)*

Approved for public release; distribution unlimited

17. DISTRIBUTION STATEMENT *(of the abstract entered in Block 20, if different from Report)*

18. SUPPLEMENTARY NOTES

19. KEY WORDS *(Continue on reverse side if necessary and identify by block number)*

Laser radar	Cross Section
Heterodyne	Target signature
Speckle	Glint
Atmospheric turbulence	

20. ABSTRACT *(Continue on reverse side if necessary and identify by block number)*

The analyses developed in a previous study (Laser Radar Analyses MDC Q0714, 15 July 1980) are modified and extended to the case of a Cassegrain laser radar receiver. A flexible computer code (LADAR) is documented that permits calculations of the degradation in heterodyne efficiency of a laser radar system that result from phase front distortions produced by target speckle effects and atmospheric turbulence. Illustrative calculations are provided to demonstrate the effects of atmospheric turbulence (for both circular aperture and Cassegrain receivers), and target speckle (conical targets and simulated aircraft are

DD FORM 1 JAN 73 1473 EDITION OF 1 NOV 65 IS OBSOLETE

UNCLASSIFIED

SECURITY CLASSIFICATION OF THIS PAGE *(When Data Entered)*

(Cont'd)

treated) on heterodyne efficiency. Efficiency calculations are also provided for a suggested test panel target to demonstrate the feasibility of using a test configuration to verify the predictions of the efficiency analyses and LADAR computer code.

FOREWORD

This report is an account of the work performed at the McDonnell Douglas Research Laboratories on Laser Radar Analyses for the Naval Surface Weapons Center, Contract No. N60921-79-C-0180, from 15 July 1980 to 15 July 1983. The work was performed in the Radiation Sciences Department by the principal investigator, Dr. J. C. Leader. Mr. J. M. Putnam was responsible for much of the computer code development. The project was monitored by Dr. R. E. Jensen, and Dr. W. J. Graham of the Naval Surface Weapons Center.

This technical report has been reviewed and is approved.

D. P. Ames
Staff Vice President
McDonnell Douglas Research Laboratories

W. J. Graham
Project Monitor
Naval Surface Weapons Center

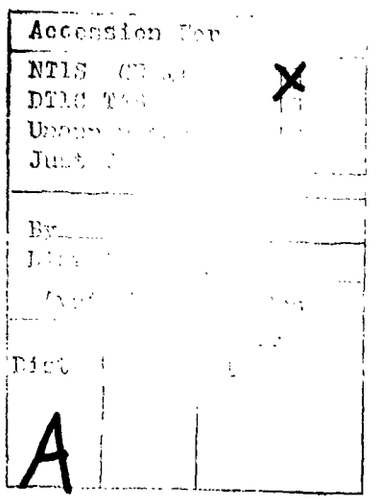

TABLE OF CONTENTS

LIST OF ILLUSTRATIONS

1. INTRODUCTION

Coherent laser detection and ranging (LADAR) systems are currently being developed for the acquisition and tracking of extended targets. Although heterodyne detection of the optical signal generally provides significant signal-to-noise ratio enhancement over incoherent detection for infrared wavelengths, the average signal (and resultant signal-to-noise ratio) may be significantly degraded by phase-front distortions resulting from target speckle and atmospheric turbulence effects, unless proper system-design precautions are observed. Similarly, monopulse tracking performance of LADAR systems can be degraded unless phase-distortion effects are understood and compensated. The objective of this study was to develop analyses and computer codes that permit reliable predictions of phase-distortion effects on heterodyne LADAR performance for realistic system parameters, target configurations, and engagement scenarios.

This final report summarizes the results obtained from 15 July 1980 through 15 July 1983 concerning the efficiency of the heterodyne-detection process resulting solely from extra-instrumental phase effects (i.e., unavoidable instrument inefficiencies are neglected). An extended period of performance was provided to permit the comparison of analytical predictions, developed under this contract, with experimental results that were to be provided under other programs. The experimental results developed during this time period were of limited value, so the emphasis of this study was re-directed toward (a) refining the analyses previously developed (MDC Final Report Q0714, Laser Radar Analyses), (b) developing and documenting a general heterodyne-efficiency prediction code, and (c) providing illustrative calculations that can be referenced for future experimental and system design activities. This report summarizes the results of these efforts.

2. SUMMARY OF RESULTS

Significant results of the contract study for the period 15 July 1980 through 15 July 1983 are summarized below. Detailed analytical results are provided in Section 5, and illustrative numerical results are given in Section 6.

- A general, flexible, computer code was developed to compute the laser-radar heterodyne-efficiency degradation that results from phase-front distortions introduced by both atmospheric turbulence and target-dependent speckle effects. The code permits speckle calculations of either a Schell-model target or a general target having an arbitrary projected cross-section distribution. Computations can be performed assuming either a circular-aperture or a Cassegrain receiver.
- A comparison of computed heterodyne-efficiency factors with experimental data obtained at the General Electric Co. (G.E.) Electronics Laboratory indicated general agreement in trends and reasonable agreement in magnitude for a diffuse scattering target but poor agreement in magnitude for a specular target. Uncertainty in experimental conditions render this comparison inconclusive.
- Good correspondence of the predictions of the computer code was demonstrated with published results of a more restrictive study that analyzed only turbulence effects coupled with restrictive receiver parameters.
- Illustrative results were computed for the speckle degradation in heterodyne efficiency that would be expected for both a simulated tactical aircraft and a Schell-model target, as a function of a range and beam radius, to emulate the detection efficiency that could be expected in an operational environment.
- A test panel configuration that could be employed for future experimental tests was developed, and efficiency computations were performed on the test array that demonstrate the feasibility of experimental tests of predictions concerning coherence effects and a phase-quadrature component.

3. CONCLUSIONS

Salient conclusions resulting from this study during the reporting period are summarized below.

- The heterodyne-efficiency computer code that was developed is sufficient for systems analyses and planned experimental tests concerning the effects of atmospheric turbulence and target speckle on the heterodyne efficiency of laser radars.
- The high confidence in the validity of the model used for heterodyne efficiency, and the resultant computer code, indicates that the lack of agreement with G.E. experimental data probably resulted from inadequately characterized experimental effects (such as beam jitter) and inadequate data acquisition and processing techniques.
- The rapid decrease in the heterodyne efficiency with decreasing range in the near-field will probably dictate either the use of focusing optics (in either transmitter or receiver) or corrective data processing to maintain a signal-to-noise ratio of a laser radar system equivalent to that at intermediate ranges.
- Predicted negative values of the laser-radar heterodyne efficiency correspond to a detected signal that is out of phase with the intermediate (heterodyne) frequency.
- The actual signal-to-noise ratio of a heterodyne laser-radar system can be increased by decreasing the transmitted beam divergence, but there exists a maximum benefit that is dependent on the particular transceiver configuration.

4. RECOMMENDATIONS

- Laser radar experiments should be conducted using the test panel configuration, suggested in Section 6.4, to verify the effects of speckle on heterodyne efficiency and the correspondence of predicted negative efficiencies with a phase-quadrature component.
- The analyses developed in this investigation should be extended to permit the study of speckle effects on monopulse tracking.
- The results of this study, which yield the effective carrier-to-noise ratio, should be integrated into a more general analysis of the complete signal-to-noise ratio, that determines the detection probability, required for acquisition studies.

5. ANALYSES

To provide a convenient reference for the equations employed in the generalized laser-radar efficiency code (section 7), relevant formulae derived in the previous investigation (Reference 1) are summarized below in Section 5.1. A corrected form of the limits of integration that arise in the incoherent form of the heterodyne-efficiency integral is provided in this summary, as well as some comments concerning the interpretation of the computed values. Section 5.2 provides a brief derivation of the modification of the heterodyne-efficiency formulae that result when the heterodyne efficiency of a receiver having Cassegrain optics is desired.

5.1 Heterodyne Efficiency Equations

Beginning with the equations for the ensemble-averaged photodetector current correlation function of a heterodyne LADAR system developed in Reference 2, the previous investigation showed that the maximum power signal-to-noise ratio heterodyne efficiency factor is given by

$$\varepsilon_{max} = \frac{S^T}{N^T}\left(\left.\frac{S^T}{N^T}\right|_{max}\right)^{-1} = \frac{\iiiint_{A_{bp}} d^2\vec{\xi}\, d^2\vec{\xi}'\ \gamma(\vec{\xi},\vec{\xi}')\ u_{\ell b}(\vec{\xi})\ u^*_{\ell b}(\vec{\xi}')}{A_r \iint_{A_{bp}} d^2\vec{\xi}\ |u_{\ell b}(\vec{\xi})|^2}, \qquad (1)$$

where γ is the spatial degree-of-coherence function at the receiving aperture plane, $u_{\ell b}$ is the normalized spatial variation of the back-propagated local-oscillator wave, A_r is the receiving aperture area, and A_{bp} is the back-propagated aperture area (i.e., the minimum areal substance of either the receiving aperture or the back-propagated local-oscillator wave, whichever is less).

To permit specific calculations of LADAR efficiency factors, the generalized transceiver system depicted in Figure 1 is considered, having the following parameters:

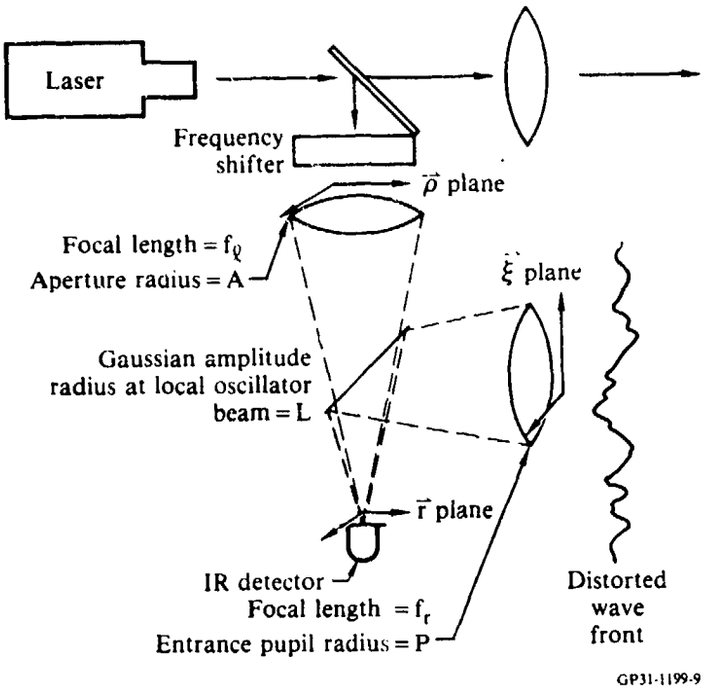

Figure 1. Transceiver parameters and coordinates.

A = local-oscillator aperture radius,

P = entrance pupil radius,

f_ℓ = focal length of local oscillator lens/mirror (lens 3), and

f_r = focal length of receiving lens/mirror (lens 2).

These parameters were used in Reference 1 to derive an excellent approximation for the back-propagated local-oscillator field using the definitions

$$z = \frac{k}{2}\left(\frac{1}{f_\ell} - \frac{1}{f_r}\right), \tag{2}$$

$$z' = z\,\frac{f_r^2}{k^2}, \tag{3}$$

and $$L'^{-2} = \frac{f_\ell^2}{f_r^2}\,L_o^{-2}. \tag{4}$$

The derived expression for the back-propagated local-oscillator field facilitates the evaluation of the heterodyne detection efficiency, Equation (1), subject to various assumptions concerning the mutual intensity functional form of the received optical signal. If the incident field correlations can be approximated by a Schell-model[3] function of the form

$$\Gamma_s(\vec{\xi},\vec{\xi}') = U_o^2 \; e^{-\frac{k}{2}(\alpha|\vec{\xi}|^2+\alpha^*|\xi'|^2)} \; e^{-|\vec{\xi}-\vec{\xi}'|^2/r_c^2} \quad , \tag{5}$$

where

$$\alpha = \frac{2}{kL_A} + \frac{i}{L_\phi} \quad , \tag{6}$$

r_c is the coherence radius, L_A is the amplitude radius, and L_ϕ is the average phase-front radius of curvature, it is straightforward to show that

$$\varepsilon_{max} = 4(\beta + \beta^*)P^{-2} \left(1 - e^{-(\beta+\beta^*)R_m^2}\right)^{-1}$$

$$\times \int_o^{R_m}\int_o^{R_m} d\xi d\xi' \xi\xi' \; I_o\left(\frac{2\xi\xi'}{r_c^2}\right) e^{-\alpha_o\xi^2-\alpha_o^*\xi'^2} \quad , \tag{7}$$

where

$$\beta = \frac{-i}{4z'} + \left(-4iz' + 16z'^2L'^{-2}\right)^{-1}, \; A' = A\, f_r/f_\ell, \; \alpha_o = \beta + \frac{k}{2}\alpha + r_c^{-2} \quad , \tag{8}$$

and

$$R_m = \begin{cases} A' \text{ if } A' < P \\ P \text{ if } P < A' \end{cases} . \tag{9}$$

Assuming an on-axis Schell-model target, the incident field correlation parameters appearing in Equations (5-8) can be calculated from the following expressions (Reference 3)

$$L_A = L_A' \left[Z^2(\rho_o^{-2} + \rho_u^{-2}) + \left|1 + i\alpha' R\right|^2 \right]^{1/2} , \tag{10}$$

$$L_\phi = R \left[Z^2(\rho_o^{-2} + \rho_u^{-2}) + \left|1 + i\alpha' R\right|^2 \right] \left[\mathrm{Im}\alpha R - |\alpha'|^2 R^2 - Z^2 \left(\tfrac{1}{2}\rho_o^{-2} + \rho_u^{-2}\right) \right]^{-1} , \tag{11}$$

and

$$r_c = Z \left[Z^2(\rho_o^{-2} + \rho_u^{-2}) + \left|1 + i\alpha' R\right|^2 \right]^{1/2} \left[\rho_o^{-2} Z^2 (1 - 2R\ \mathrm{Im}\ \alpha + |\alpha'|^2 R^2) \right.$$

$$\left. + \rho_o^{-2}\ Z^2 (R\ \mathrm{Im}\alpha' + \tfrac{3}{4} Z^2 \rho_o^{-2}) + \rho_u^{-2}\ Z^2 (1 + \rho_o^{-2} Z^2) \right]^{-1/2} , \tag{12}$$

where α', appearing in Equations (10-12), is the Equation (6) parameter that results from the target amplitude and phase-front radii (L_A' and L_ϕ'), R is the target range, and ρ_o and ρ_u are the atmospheric and target coherence lengths, respectively.

A more general expression for the heterodyne detection efficiency is obtained by relaxing the constraint that the target radiance is Gaussian (yielding the Equation (5) functional form for the mutual intensity). If the target has a single glint point and an arbitrary diffuse reflectivity distribution, the degree-of-coherence function will be given by[1]

$$\gamma(\vec{\xi}^{+}, \vec{\xi}^{-}) = e^{-ik\,R^{-1}\,\vec{\xi}^{+}\cdot\vec{\xi}^{-}}\; e^{-|\vec{\xi}^{-}|^2/\rho_o^2}\left[\pi a_1 a_2 + \Lambda \iint_{-\infty}^{\infty} d^{2\vec{p}}\; e^{\frac{ik}{R}\,\vec{p}\cdot\vec{\xi}^{-}}\;\frac{d^2\sigma(\vec{p})}{d\vec{p}^{2}}\right]$$

$$\times\left[1 + \Lambda \iint_{-\infty}^{\infty} d^{2\vec{p}}\;\frac{d^2\sigma(\vec{p})}{d\vec{p}^{2}}\right]^{-1}, \qquad (13)$$

where

$$\vec{\xi}^{+} = \frac{1}{2}\,(\vec{\xi} + \vec{\xi}'), \quad \vec{\xi}^{-} = \vec{\xi} - \vec{\xi}',$$

R = range to target,

$\vec{p}$ = transverse coordinate to line-of-sight at the target plane,

$\frac{d^2\sigma(\vec{p})}{d\vec{p}^{2}}$ = differential projected scattering cross-section per unit area,

a_1 and a_2 are the Gaussian radii of curvature at the glint point, Λ is a factor that relates the relative strength of the coherent (glint) and incoherent components, and the denominator of Equation (13) results from the normalization requirement of the degree-of-coherence function.

The parameter ρ_o in Equation (13) is the turbulent-atmosphere spherical-wave coherence length $\left[\rho_o = [3/8 \times 1.455\; k^2 R C_n^2]^{-3/5}\right.$, where C_n^2 is the refractive index structure constant$\left.\right]$ describing the effect of the assumed homogeneous atmospheric turbulence on the propagation of partially coherent light.[4]

Recognizing that the generalized degree-of-coherence function of Equation (13) consists of the sum of a coherent and incoherent component, the calculated heterodyne-efficiency factor, given by Equation (1), likewise can be split into the sum of two components. The maximum heterodyne efficiency can be expressed as

$$\varepsilon = \varepsilon_{coh}(1 + \Lambda\sigma_{tar}/\pi a_1 a_2)^{-1} + \varepsilon_{incoh}(1 + \pi a_1 a_2/\Lambda\sigma_{tar})^{-1}, \qquad (14)$$

where σ_{tar} is the total target incoherent LRCS, i.e.,

$$\sigma_{tar} = \iint_{-\infty}^{\infty} d^2\vec{p}\, \frac{d^2\sigma(\vec{p})}{d\vec{p}^2} \tag{15}$$

and the coherent and incoherent efficiencies are determined from the relation

$$\varepsilon_{coh/incoh} = \frac{2\beta_r\, Q_{coh/incoh}}{(\pi P)^2} \left(1 - e^{-R_m^2(\beta+\beta^*)}\right)^{-1} . \tag{16}$$

the integral factors $Q_{coh/incoh}$ are defined by the integral numerator of Equation (1). Because the coherent component of the degree-of-coherence function is in the form of a Schell-model MIF, the coherent component of the total efficiency can be expressed in the form of Equation (7) with the variable α_o replaced by the variable α_1 defined as

$$\alpha_1 = i\left\{\frac{k}{2R} + \frac{4z'L'^{-4}}{[1 + (4z'L'^{-2}]}\right\} + \rho_o^{-2} . \tag{17}$$

The incoherent integral factor can be written in the form

$$Q_{incoh} = \frac{1'}{2} \iint_{-\infty}^{\infty} d^2\vec{\xi}^{+} e^{-2\beta_r \vec{\xi}^{+2}} \Theta(R_m^2 - \vec{\xi}^{+2}) \iint_{-\infty}^{\infty} d^2\vec{\zeta}' \, \tilde{F}\left[kR\ (\zeta'^{-1} \vec{\xi})\right] \frac{d^2\sigma(-\vec{\zeta}')}{d\vec{\zeta}'^2} , \tag{18}$$

where

$$\vec{\zeta}' = Rk^{-1}\vec{\mu}' , \quad \vec{\zeta} = \vec{\xi}^{+} (1 + 2Rk^{-1}\beta_1), \tag{19}$$

$$\tilde{F}(\tilde{\mu}') = \frac{4\pi\sqrt{R_m^2 - \vec{\xi}^{+2}}}{\tilde{\beta}} e^{-\vec{\mu}'^2/2\tilde{\beta}} \int_o^{\infty} d\mu'' J_1\left[\mu''\, 2\sqrt{R_m^2 - \vec{\xi}^{+2}}\right] I_o(\vec{\mu}'\mu''/\tilde{\beta})\, e^{-\vec{\mu}''^2/2\tilde{\beta}} , \tag{20}$$

and $\tilde{\beta} = \beta_r + 2\rho_o^{-2}$, (21)

by transforming the integration limits of Equation (14) to the sum and difference coordinates and utilizing the convolution integral expression for the Fourier transform of the product of two functions. The notations β_r and β_i employed in the above expressions denote the real and imaginary parts of β, respectively. The function $\tilde{F}(\vec{\mu}')$ defined by Equation (20) results from the Fourier transform of the turbulent-atmosphere spherical-wave MIF truncated by the finite receiver aperture limits and Gaussian local-oscillator field distribution.[2] Physically, $\tilde{F}$ represents the spatial filtering of the target's spatial power spectrum by the turbulent atmosphere and finite limits of the receiver. The Equation (20) expression for the filtering function, $\tilde{F}$, differs from that reported in Reference 1 (Equation 68). The corrected expression, Equation (20), reflects the fact that the sum and difference coordinates

$$\vec{\xi}^{+} = \frac{1}{2}(\vec{\xi} + \vec{\xi}')$$

and

$$\vec{\xi}^{-} = \vec{\xi} - \vec{\xi}' \tag{22}$$

can be expressed in terms of the aperture coordinates $\vec{\xi}$ and $\vec{\xi}'$ to yield a restriction on their combined limits, viz.,

$$2\vec{\xi}^{+2} + \frac{1}{2}\vec{\xi}^{-2} = \vec{\xi}^{2} + \vec{\xi}'^{2} \leq 2R_m^2. \tag{23}$$

Thus, the difference coordinate, that is the integration variable in the inner integral of Equation (18), is restricted to the range

$$\vec{\xi}^{-2} \leq 4(R_m^2 - \vec{\xi}^{+2}), \tag{24}$$

which is reflected in the parameters appearing in the filter function in Equation (20).

To numerically evaluate Equation (18), it is desirable to employ an approximate analytical form for the filtering function $\tilde{F}$. It is demonstrated in Reference 1 that an excellent approximation to Equation (20) results from the function

$$F(\vec{\mu}') = \begin{cases} \tilde{F}_{sp}(\mu') & \mu' > \tilde{\beta}D \\ \tilde{F}_{E}(\mu') & \mu' < \tilde{\beta}D \end{cases} , \tag{25}$$

where

$$\tilde{F}_{sp}(\mu') = 2\pi D^2 \frac{J_1(\mu' D)}{\mu' D} \tag{26}$$

and

$$\tilde{F}_{E}(\mu') \cong 2\pi \left[e^{-\frac{1}{2}\mu'^2/\tilde{\beta}} (\tilde{\beta})^{-1} - e^{-\frac{1}{2}D^2(\tilde{\beta}+\frac{1}{2}\mu'^2)} (\tilde{\beta}+\frac{1}{2}\mu'^2)^{-1} \right] . \tag{27}$$

The parameter Γ appearing in Equations (25)-(27) is the integration limit of the difference coordinate, i.e.,

$$D = 2\sqrt{R_m^2 - \vec{\xi}^{+2}} , \tag{28}$$

which replaces the back-propagated aperture radius, R_m, in the corresponding expression (Equations (79)-(72)) of Reference 1. It should also be noted that Equation (18) differs from Equation (67) of Reference 1 by a factor of 1/2. This factor results from the observation that because

$$\vec{\xi} = \vec{\xi}^{+} + \frac{1}{2}\vec{\xi}^{-}$$

and

$$\vec{\xi}' = \vec{\xi}^{+} - \frac{1}{2}\vec{\xi}^{-} , \tag{29}$$

when $\vec{\xi}^{-}$ is transformed to $-\vec{\xi}^{-}$, the aperture coordinates of Equation (29) are interchanged. Thus, a circularly symmetric integration over the variable $\vec{\xi}^{-}$ in Equation (18) yields a double mapping over the coordinates $\vec{\xi}$ and $\vec{\xi}'$.

It is easy to demonstrate, using the approximate forms for the filter function, that the incoherent detection efficiency approaches unity as R_m goes to zero and approaches zero in a limiting fashion as R_m goes to infinity, as required from the physics of the problem. Computed results presented in Section 6.2 demonstrate the correspondence of the general expression, Equation (18), with the more restrictive formula, Equation (7), for the special case of a Schell-model source. The resultant confidence in the approximations employed for the spatial filtering function, $\tilde{F}$, coupled with the comparisons of the preceding analyses[5] with independent investigations of a more limited scope[6], support the validity of Equations (18), (19), and Equations (25)-(27). These formulae provide a prescription for calculating the heterodyne efficiency of detecting a target of rather arbitrary laser-reflectivity properties in the presence of atmospheric turbulence. Although other investigators have performed extensive analyses of the signal-to-noise degradation of laser-radar imagery resulting from speckle effects and atmospheric turbulence[7], a similar investigation of heterodyne efficiency has not been heretofore reported.

The user of the above formulae should note several points concerning their derivation and interpretation. First, the derivation assumes that the mutual intensity function (which is a statistical measure derived from an ensemble average) adequately describes the time-averaged phase-front correlations that give rise to the time-averaged laser-radar signal. This assumption is predicated on a form of the ergodic hypothesis[8] which holds when the phase deviations produced by the scattering are large and the scattered field is quasihomogeneous so that a spatial average samples the stochastic variations of the system. In this event, the spatial variations of the scattering geometry that change with time, encountered for most laser-radar systems, yield time-averaged signals that should be in good accord with the prediction of an ensemble-averaged statistic. Second, the derivation is predicated on the frequency integrated signal power which is given by the current variance.[1] Thus, the derived relations describe the heterodyne efficiency for the signal power included in all spectral components of the laser-radar pulse-form when the pulse is "on". Finally, it should be noted that the numerator of the derived expression for the heterodyne signal-power efficiency, Equation (1), is such that negative values are possible. The fact that negative values of the mutual intensity function can dominate the inte-

grated contribution is evident from the Equation (13) form of the degree-of-coherence function, which shows that the incoherent contribution can be presented in the form of a Fourier transform of the differential projected scattering cross-section. Clearly, negative values of the Fourier transform are permissable and, in fact, this eventuality is demonstrated in a numerical example provided in Section 6. The calculated negative values, however, pose a problem concerning their physical interpretation because the calculated quantity is a power ratio which should always be positive. Because the derivation[2] assumes that the heterodyne current is at the heterodyne intermediate frequency (i.e., in phase with the difference frequency between the laser and local oscillator), it seems reasonable to assume that negative values correspond to the out-of-phase (quadrature) component. This interpretation is supported by the reasonable physical predictions obtained assuming a physically meaningful power value for negative values presented in Figure 14 in Section 6. The verification of this physical interpretation of the negative efficiencies as a quadrature component must, however, await further experiments.

5.2 Cassegrain Receiver Geometry

The equations summarized in the preceding section were developed for the laser-radar system depicted in Figure 1, where an unobstructed, circularly symmetric, receiver collects the laser light scattered from the target through the turbulent atmosphere. Because the phase-front distortion effects on the heterodyne efficiency are calculated from the phase interference with the back-propagated local-oscillator wave at the receiver aperture, the foregoing equations must be modified to treat the case of a Cassegrain receiver where a central area of the receiving aperture is obscured. The following development treats the necessary modifications for the Cassegrain receiver that are implemented in the general heterodyne-efficiency code listed in Section 7.

Because all of the heterodyne-efficiency equations are of integral form, since they are derived from the basic integral equation given in Equation (1), it is sufficient to consider a general integrand of two spatial variables, $f(\vec{r}, \vec{r}')$, integrated between limits R_I and R_O representing the inner obscuration radius and the outer aperture radius, respectively. It is straightforward to show that

$$\int_{R_i}^{R_o}\int_{R_i}^{R_o} d^2\vec{r}d^2\vec{r}'\, f(\vec{r},\vec{r}') = \int_{o}^{R_o}\int_{o}^{R_o} d^2\vec{r}d^2\vec{r}' f(\vec{r},\vec{r}') + \int_{o}^{R_i}\int_{o}^{R_i} d^2\vec{r}d^2\vec{r}' f(\vec{r},\vec{r}')$$

$$- 2\int_{o}^{R_i}\int_{o}^{R_o} d^2\vec{r}d^2\vec{r}' f(\vec{r},\vec{r}'). \qquad (30)$$

Thus, the integral expression for the Schell-model target heterodyne efficiency, Equation (7), and the coherent component heterodyne efficiency (Equation (17) with Equation (7)) can be calculated for a Cassegrain receiver geometry using the Equation (30) prescription for the limits of integration appropriate for the receiver. It is also straightforward to show that the efficiency integral is normalized by a factor given by

$$\varepsilon_{coh/incoh} = \frac{2\beta_r}{\pi^2(P_o^2 - P_i^2)}\left[e^{-R_{mi}^2(\beta+\beta^*)} - e^{-R_{mo}^2(\beta+\beta^*)}\right]^{-1} \qquad (31)$$

instead of Equation (16) in the case of Cassegrain receiver. The notation employed in Equation (31) is a subscript form of the parameters defined earlier, viz., P_o and P_i are the outer aperture radius and inner aperture radius, respectively, and R_{mi} and R_{mo} are the respective inner and outer back-propagated local-oscillator beam radii (i.e., the extension of Equation (9) to the Cassegrain geometry).

Although Equations (30) and (31) suffice to adapt the previous formulae for Schell-model targets and the coherent component of scattering, the limits of integration of the incoherent component, Equation (18), must be further modified because this equation is given in terms of the sum and difference coordinates. It is clear from the above development that the limits of integration on three integrals must be determined in terms of the sum and difference coordinates for the incoherent scattering contribution for Cassegrain geometries, however the development provided below demonstrates that the consideration of the mixed limits integral (the last integral in

Equation (30)) suffices to provide the limits on the previous two integrals. The mixed limits integral of two spatial variables can be written

$$\int_0^{R_o}\int_0^{R_i} d^2\vec{\xi}\,d^2\vec{\xi}'\; f(\vec{\xi},\vec{\xi}') = \iint_{-\infty}^{\infty} d^2\vec{\xi}\,d^2\vec{\xi}\; f(\vec{\xi},\vec{\xi}')\;\Theta\left(R_o^2 - \vec{\xi}^{\,2}\right)\Theta\left(R_i^2 - \vec{\xi}'^{\,2}\right) \tag{32}$$

in terms of the aperture coordinates and the Heaviside functions, Θ. Because of the relations (Equation (22)), between the aperture coordinates and the sum and difference coordinates, it follows that

$$2\vec{\xi}^{+2} + \frac{1}{2}\vec{\xi}^{-2} = \vec{\xi}^{2} + \vec{\xi}'^{2} \leq R_o^2 + R_i^2 \tag{33}$$

for the mixed limits of integration case, so that

$$\vec{\xi}^{-2} \leq 4\left(\bar{R}^2 - \vec{\xi}^{+2}\right), \tag{34}$$

where

$$\bar{R}^2 = \frac{1}{2}\left(R_o^2 + R_i^2\right) . \tag{35}$$

In a similar manner, the defining equations may be used to show that

$$\vec{\xi}^{+2} = \frac{1}{4}\left(\vec{\xi}^{2} + \vec{\xi}'^{2} + 2\vec{\xi}\cdot\vec{\xi}'\right), \tag{36}$$

so

$$\vec{\xi}^{+2} \leq \frac{1}{4}\left(R_o^2 + R_i^2 + 2R_o\,R_i\right) = R^{+2}, \tag{37}$$

where

$$R^{+} = \frac{1}{2}\left(R_o + R_i\right). \tag{38}$$

Therefore, the mixed integration limits integral may be written

$$\int_0^{R_o}\int_0^{R_i} d^2\vec{\xi}\, d^2\vec{\xi}'\, f(\vec{\xi}, \vec{\xi}') = \iint_{-\infty}^{\infty} d^2\vec{\xi}^{+}\, d^2\vec{\xi}^{-}\, f(\vec{\xi}^{+}, \vec{\xi}^{-})\, \Theta\,(R^{+2} - \vec{\xi}^{+2})$$

$$\times\, \Theta\left[4(\bar{R}^2 - \vec{\xi}^{+2}) - \vec{\xi}^{-2}\right] \tag{39}$$

in terms of the sum and difference coordinates. Equations (35), (38), and (39) show that the incoherent efficiency scattering integral reduces to the form previously derived for an unobscured aperture when the outer and inner integration limits are equal. Thus, the first two integrations reduce to the case previously treated, Equations (18) and (20), with R_m replaced by R_{mi} and R_{mo} respectively. For the case of mixed integration limits, Equations (18) and (20) become

$$Q_{incoh} = \frac{1}{2} \iint_{-\infty}^{\infty} d^2\xi^{+} e^{-2\beta_r \vec{\xi}^{+2}}\, \Theta(R^{+2} - \vec{\xi}^{+2}) \iint_{-\infty}^{\infty} d^2\vec{\zeta}'\, \tilde{F}\left[kR^{-1}(\vec{\zeta}' - \zeta)\right] \frac{d^2\sigma(-\vec{\zeta}')}{d\vec{\zeta}'^2} \tag{40}$$

and

$$\tilde{F}(\tilde{\mu}') = \frac{4\pi\sqrt{\bar{R}^2 - \vec{\xi}^{+2}}}{\tilde{\beta}}\, e^{-\vec{\mu}'^2/2\tilde{\beta}} \int_0^{\infty} d\mu'' J_1\left[\mu''\, 2\sqrt{\bar{R}^2 - \vec{\xi}^{+2}}\right] I_o(\vec{\mu}'\mu''/\tilde{\beta})\, e^{-\vec{\mu}''^2/2\tilde{\beta}}\,, \tag{41}$$

respectively. The above equations provide the basis for the modifications included in the laser-radar heterodyne-efficiency code of Section 7 that permit Cassegrain receiver efficiences to be calculated when that option is selected.

6. NUMERICAL RESULTS

To illustrate the effects of atmospheric turbulence and speckle on heterodyne detection-efficiency, several efficiency functional dependencies are provided below that were numerically computed from the equations summarized in the previous section as implemented in the generalized efficiency code presented in the subsequent section. Specifically, Section 6.1 provides a comparison of the calculated results with the only applicable experimental data that has been measured to date, and Sections 6.2 and 6.3 provide calculated results for atmospheric turbulence degradations of efficiency for a clear aperture receiver and a Cassegrain receiver, respectively. Section 6.4 provides calculated results of the speckle-related degradation in heterodyne efficiency for a conical target, a representative tactical aircraft target, and a test-panel configuration that could be employed for subsequent tests.

6.1 Comparison of Calculated and Experimental Results

Laser-radar heterodyne-efficiency factors were calculated for the G.E. laser-radar experimental parameters employed on 13 July 1981 test.[9] Assumed parameters of the calculations were chosen to emulate the G.E. experimental parameters (i.e., local-oscillator aperture radius = 0.043 m, Cassegrain obscuration radius = 0.025 m, Cassegrain outer radius = 0.0381, 0.0509, 0.0762, 0.0889, and 0.0953 m, receiver focal length = 3.05 m, local-oscillator focal length = 4.06 m, local-oscillator beam radius = 0.1 m, target range = 609 m, and transmit beam divergence = 0.6 mrad). The local-oscillator aperture radius was chosen to emulate the finite size of the infrared detector that was effectively flooded with the local-oscillator beam radiation. A Schell-model (Gaussian) target intensity distribution was assumed for the diffuse target because the transmitted beam was presumeably a TEM_{00} mode and the target was flat and uniformly diffuse. The calculated results are compared with the experimental data in Figure 2 as a function of the Cassegrain aperture diameter. It is apparent that the calculated results for the glint target exceed measured values, while the diffuse target predictions are somewhat less than measured results, although both predictions follow

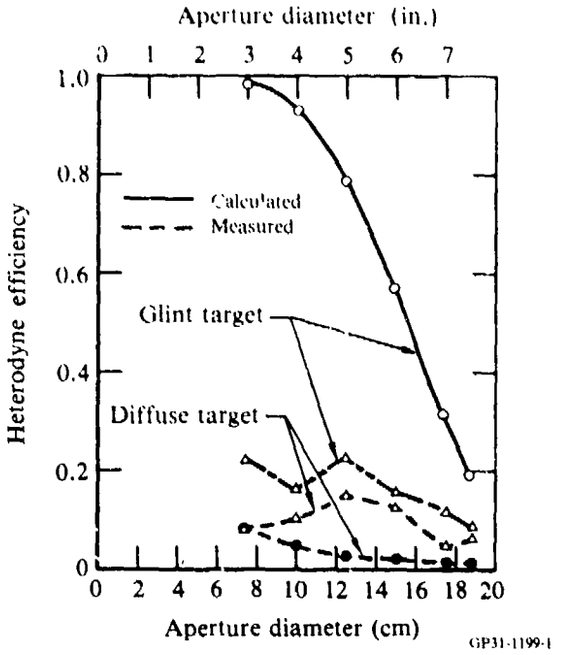

Figure 2. Calculated and measured laser-radar heterodyne efficiency factors for the G.E. laser-radar experimental parameters employed on the 13 July 1981 tests.

observed trends (i.e., they decrease with increasing Cassegrain aperture size because of near-field effects). The diffuse target results would be closer to observed data if a smaller beam divergence were assumed. It is noteworthy that Reference 9 emphasizes that the beam divergence is one of the most ill-determined parameters of the experiment, the other being the absolute heterodyne efficiency. Although Figure 2 would indicate that the diffuse target calculations are in better accord with the experimental data, it is apparent that systematic errors are present in the data that preclude a valid comparison. These errors are evident by the fact that (1) a near-unity heterodyne efficiency was not measured for the case of the glint target with minimum aperture and (2) both the glint and diffuse target efficiencies show an anomalous rise for the 5 in. aperture case. Both of the aforementioned experimental anomalies cannot be rationalized with the known physics of the detection process. It is possible that beam-jitter problems adversely affected the optical alignment, resulting in lower measured heterodyne efficiencies for the glint target. The diffuse target measurements would not be as subject to beam-jitter problems because of the diffuse target

scattering, however, the speckle effects that result from diffuse scattering require careful data recording and statistical analyses that were not adequately performed in the Reference 9 study. Although the experimental data generally support the predicted trends, the obvious introduction of artifacts renders the comparison inconclusive.

6.2 Turbulence Effects on a Circular Aperture Heterodyne Receiver

Clifford and Wandzura[6] have performed calculations of the effects of the turbulent atmosphere on heterodyne laser-radar performance assuming a focused beam wave, but ignoring the effects of a finite collection aperture. To demonstrate the correlation of the predictions of this analysis with the results of Clifford and Wandzura, Figure 3 shows computed efficiencies as a function of integrated turbulence, assuming the unlikely conditions of Reference 6, where the aperture size is much larger than the Gaussian beam radius. The integrated turbulence number as defined by Clifford and Wandzura is

$$N_o = \frac{\sqrt{2}\, L_o}{\rho_o} , \tag{37}$$

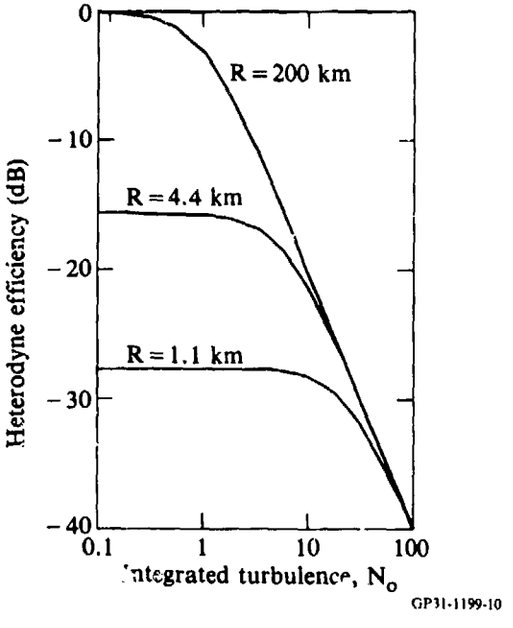

Figure 3. Calculated heterodyne efficiency as a function of integrated turbulence. Calculations assume $A = P = 5$ m, $L_0 = 0.3$ m, $f_\ell = f_r = 0.5$ m, and $\lambda = 10.6$ μm.

where the factor of $\sqrt{2}$ results from the different definitions of the Gaussian beam radius employed in their investigation and this one. Figure 3 depicts the functional dependence of the heterodyne efficiency on the integrated turbulence for three different range values corresponding to the Fresnel numbers ($\Omega = kL_o^2/R$) of approximately 0, 4, and 16 used in the Reference 6 calculations. The Figure 3 results were computed from Equations (7) and (17) and agree with the results calculated by Clifford and Wandzura using the quadratic atmospheric structure-function approximation[4] assumed in this work. However, these results differ slightly from results computed assuming the more exact five-thirds power-law atmospheric structure function, as pointed out in Reference 6. Larger Fresnel numbers delay the decrease of the heterodyne efficiency with increasing turbulence, although the initial efficiency is lower because of near-field effects (i.e., poor phase matching on the photo-detector).

Figure 4 shows efficiency calculations similar to that of Figure 3; however, the receiver aperture was assumed to be the same size as the local-oscillator beam radius for these computations. Figures 3a and 3b differ only in their method of computation: Figure 3a was computed from Equations (7) and (17), whereas Figure 3b was computed from the more general Equations (16), (18), and (20), assuming a point-like reflecting object having a radius of only 1 mm. The discrepancies between Figures 4a and 4b result solely from numerical inaccuracies in computing the filter function of Equation (20). Numerical computations of the filter function become increasingly difficult for larger Fresnel numbers (Ω), and the approximations of Equations (25)-(27) also become invalid. The Figure 4 results are particularly interesting because they indicate that the finite receiving aperture has the effect of further delaying the decrease of the efficiency with increasing turbulence compared with the beam-wave local-oscillator case of Figure 3, and a small increase of heterodyne efficiency is noted for certain integrated turbulence values for large Fresnel numbers. Remarkably, the more-accurate Figure 4a results replicate the calculations of Clifford and Wandzura for the beam-wave local-oscillator configuration using the more-accurate assumption of a five-thirds power-law atmospheric structure function, although a quadratic structure function was assumed for these computations. Clifford[10] explains the increase in heterodyne efficiency for large Fresnel numbers and certain

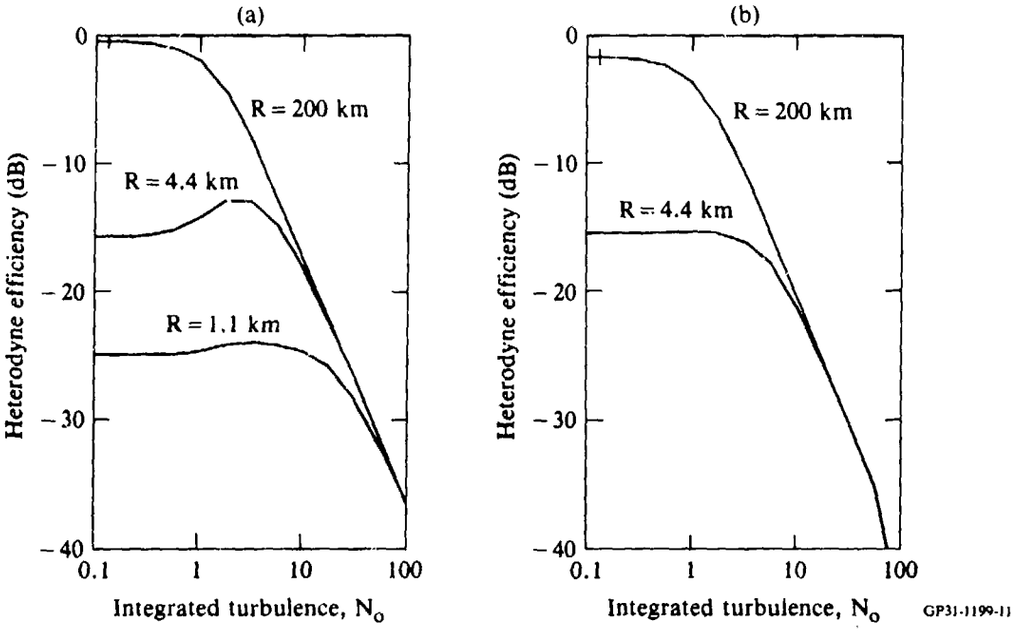

Figure 4. Calculated heterodyne efficiency as a function of integrated turbulence. Calculations assume $A = P = L_0 = 0.3$ m, $f_Q = f_r = 0.5$, and $\lambda = 10.6$ μm. Figure 4a is computed from Eqs. (7) and (17) and Fig 4b is computed from Eqs. (18) and (25).

turbulence strengths as resulting from signal increases caused by the focusing effect of large-scale turbulent eddies. This explanation, however, must be re-examined because of the correspondence of Figure 4a with the Reference 6 results and the differences between Figures 3 and 4.

6.3 Turbulence Effects on a Cassegrain Heterodyne Receiver

To illustrate the effect of a Cassegrain receiver geometry (a customary LADAR design) on heterodyne detection efficiency, Figure 5 shows the efficiency reduction with increasing integrated turbulence for the same conditions assumed in Figure 4 obscuration having a radius of 20 cm. The Figure 5 results, calculated from Equations (7), (17), (30) and (31), indicate that the central obscuration generally has the effect of increasing the heterodyne efficiency over a similarly configured unobscured receiver, although anomalies are apparent for the high Fresnel number calculation (Ω = 16, R = 1.1 km). This conclusion is expected because of the larger relative size of the coherence length with respect to the unobscured aperture dimension. If the

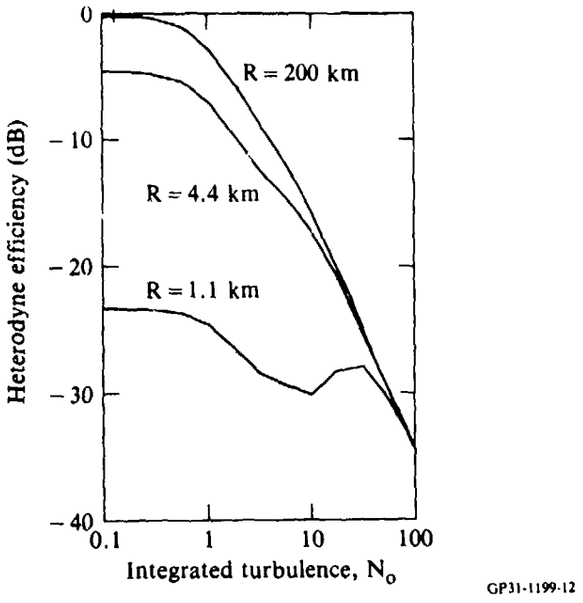

Figure 5. Calculated heterodyne efficiency as a function of integrated turbulence for a Cassegrain receiver geometry. Calculations assume $A = L_0 = 0.3$ m, $f_\ell = f_r = 0.5$ m, $\lambda = 10.6$ μm, and an inner (obscuration) radius of $P_{in} = 0.2$ m and outer (receiver aperture) radius of $P_{out} = 0.3$ m.

integrated turbulence number, N_o, is redefined to more accurately reflect the integration area of the Cassegrain receiver, the apparent benefits of a Cassegrain geometry disappear.

6.4 Speckle Effects on Heterodyne Efficiency

Conical-Target Scattering

Numerous calculations have been performed using the analyses summarized in Section 5 to assess the effects of phase-front distortions resulting from target speckle on the heterodyne efficiency. Illustrative of the types of speckle effects that are encountered are the cone scattering efficiency calculations shown in Figure 6. The Figure 6 data show the variation in heterodyne efficiency as a function of the aspect angle of a conical target having a metallic rough surface such that the bidirectional reflectivity of the surface is that shown in Figure 7. The assumed bidirectional reflectivity function is typical of many rough surfaces and was used to calculate the projected conical-target cross section per unit area ($d^2\sigma/d\vec{p}^2$) with the aid of

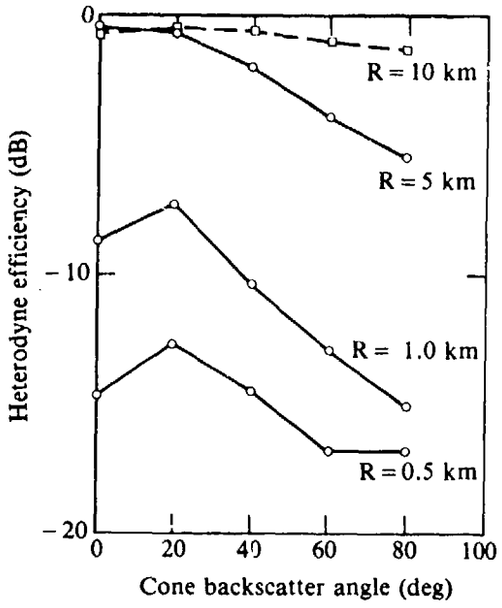

Figure 6. Calculated heterodyne-detection efficiency as a function of viewing angle for a conical target having a base radius of 0.25 m, a height of 1.0 m, and a surface finish characterized by the bidirectional reflectivity distribution depicted in Fig. 7. The fixed parameters of the calculation are A = P = 2.5 cm, $f_\ell = f_r = 25$ cm, $L_0 = 5$ cm, $C_n^2 = 10^{-14}$ $m^{-2/3}$, and range (R) values are annotated.

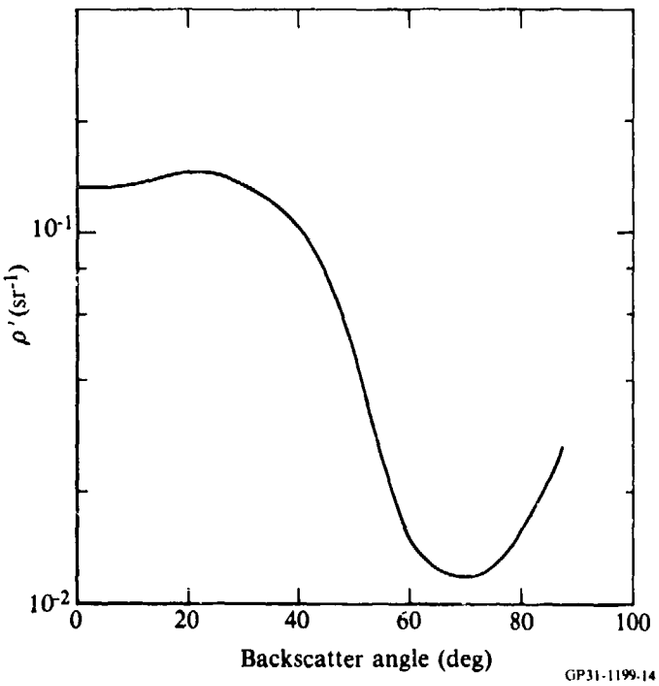

Figure 7. Laser backscatter bidirectional distribution functions for hypothetical metallic rough-surface materials having two scales of roughness characterized by the ROSSCO parameters; $k\sigma = 0.2$, $kH = 5.0$, $k\ell = 3.0$, $s = 0.6$, $m = 1.0$, $n = 100.0$, and $\alpha = 0$.

the ROSSCO code summarized in Reference 11. The heterodyne efficiencies, plotted in Figure 6 for various ranges, were computed from Equations (18), (25), (26), and (27) using the four-fold numerical integration employed in the generalized efficiency code of Section 7 that has been shown to be convergent. The Figure 6 data differ slightly from the corresponding results depicted in Figure 25 of Reference 1 because of the modified integration limits employed in the more recent calculations, although the magnitude and trends of the two sets of calculated data are similar, verifying the modest effect of the changed integration limits on the calculated results. The Figure 6 data basically depict the decrease in heterodyne efficiency with increasing projected target-radiance solid-angular subtense (resulting in a smaller radial coherence length). It is also clear from the longer-range data of Figure 6 (note the crossing of the R = 5 km and R = 10 km data) that atmospheric turbulence eventually becomes the dominant factor in determining the efficiency after the solid angle is reduced sufficiently. Thus there is an optimum range for maximum detection efficiency depending upon the target characteristics and turbulence conditions.

Tactical Aircraft Simulation

To provide an indication of the heterodyne detection efficiencies that might be expected in a more realistic laser-radar detection scenario, efficiency calculations were performed using the simulated, tactical aircraft, projected cross-section depicted in Figure 8. The Figure 8 cross-section distribution assumes a spatially constant laser bidirectional reflectance function of $\rho' = 5 \times 10^{-3}$ sr^{-1} which corresponds to the sample D of Reference 11 (green paint on metal) at a backscatter angle of 70^{o}. This reflectance function yields a total target cross section of 48 cm^2. For calculational purposes, the target distribution of Figure 8 was discretized into a 20 x 20 grid and calculations were performed as a function of range, Figure 9, for the fully illuminated target and as a function of beam size, Figure 10, at 4 km. The transceiver parameters were those employed for many of the previous calculations and were chosen to be representative of a compact installation.

Two simple range proportionalities (R and R^4) are depicted in Figure 9 to illustrate the fact that the heterodyne-efficiency range dependence decreases more rapidly than R^4 for close ranges, increases less rapidly than

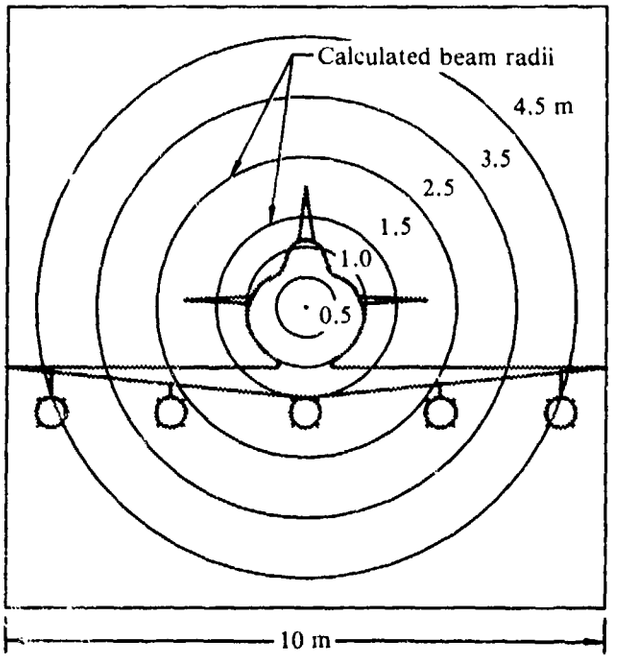

Figure 8. Simulated tactical aircraft nose-on projected cross-section The laser bidirectional-reflectance function is assumed to be $\rho' = 5 \times 10^{-3}$ sr^{-1}. The superimposed anulii represent the assumed illuminating-beam radii used for heterodyne efficiency calculations.

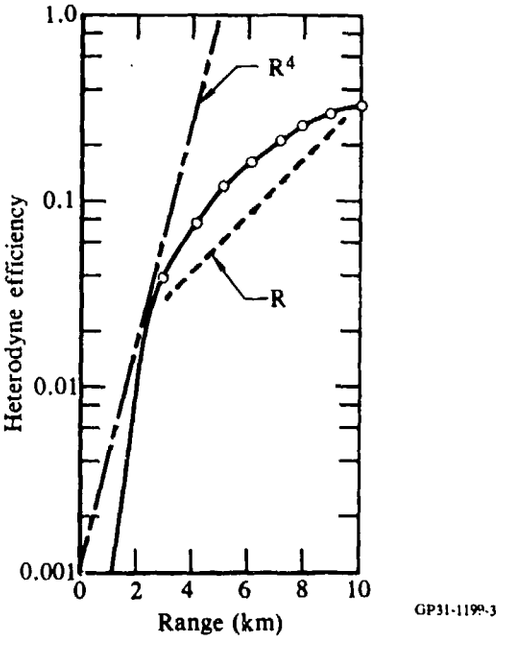

Figure 9. Calculated heterodyne-detection efficiency as a function of range for the simulated tactical aircraft target depicted in Fig. 8. Straight lines indicate the slopes of efficiencies proportional to R and R^4 as indicated. The fixed parameters of the calculation are A = P = 2.5 cm, $f_\ell = f_r = 25$ cm, $L_0 = 5$ cm, $\lambda = 10.6$ μm, and $C_n^2 = 10^{-14} m^{-2/3}$.

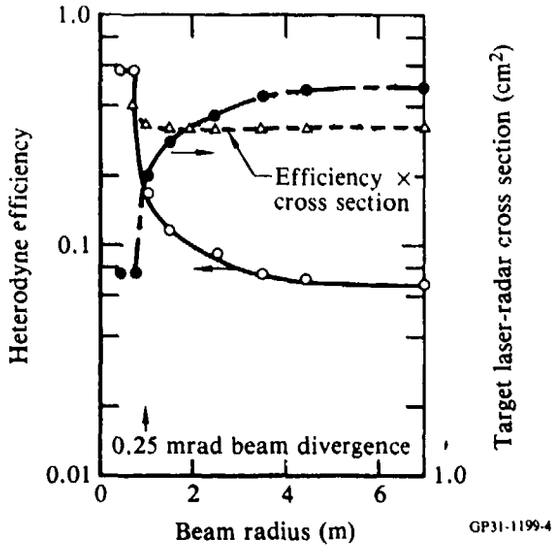

Figure 10. Calculated heterodyne-detection efficiency as a function of illuminating-beam radius for the simulated tactical aircraft target depicted in Fig. 8. The fixed parameters of the calculation are $A = P = 2.5$ cm, $f_\ell = f_r = 25$ cm, $L_0 = 5$ cm, $\lambda = 10.6$ μm, $C_n^2 = 10^{-14}$ $m^{-2/3}$, and $R = 4$ km. The illuminated-area laser-radar cross section is plotted and the product of the calculated heterodyne efficiency and laser-radar cross section is shown as a relative magnitude.

R for long ranges, and cannot be modeled by a simple power relationship, as one might expect from a simple coherence area argument. The rapid decrease in heterodyne efficiency for close ranges implies that focusing optics may be required for an operational large-aperture system to maintain an acceptable signal-to-noise ratio because the signal increase with decreasing range will be proportional to only R^4 (as a result of the radar range equation). The net decrease in signal-to-noise ratio that Figure 9 implies for close ranges may be unacceptable for certain applications. Because the typical dimensionality of a speckle cell decreases inversely with the range (if the target is quasi-homogeneous) one might expect that the efficiency should decrease inversely with R^2 because the efficiency is related to the integral of the coherence area (Equation (1)); however, Figure 9 shows that this is not the case. Also, Figure 9 shows that because of the large extent of the target, a unity heterodyne efficiency is not achieved at any range because turbulence effects become important at the ranges where the target speckle effects become unimportant (> 10 km). Although efficiencies at ranges greater than 10 km are not shown in Figure 9, the efficiency decreases at ranges much greater than 10 km because of atmospheric turbulence.

Figure 10 demonstrates that the heterodyne efficiency can be increased by decreasing the illuminated target area; however, the converse behavior of the laser-radar cross section, also plotted in Figure 10, demonstrates that the net gain is modest. Because the actual signal-to-noise ratio is proportional to the product of the heterodyne efficiency and the signal power (which is proportional to the laser-radar cross section), the product of the heterodyne efficiency and laser-radar cross section is plotted in Figure 10 to illustrate the relative actual signal-to-noise ratio. The Figure 10 results indicate that the actual signal-to-noise ratio does not decrease beyond a beam divergence angle of 0.25 mrad. It should be noted that the constant values of heterodyne efficiency and laser-radar cross section indicated for the smallest values of beam radius, result from the finite discretization of the target cross section distribution and are not physically meaningful.

To demonstrate that the general trends illustrated in Figures 9 and 10 are not unique to the target geometry assumed for the calculations, corresponding results are shown in Figures 11 and 12 for a Schell-model target that would correspond to a uniform diffuse target illuminated with a Gaussian

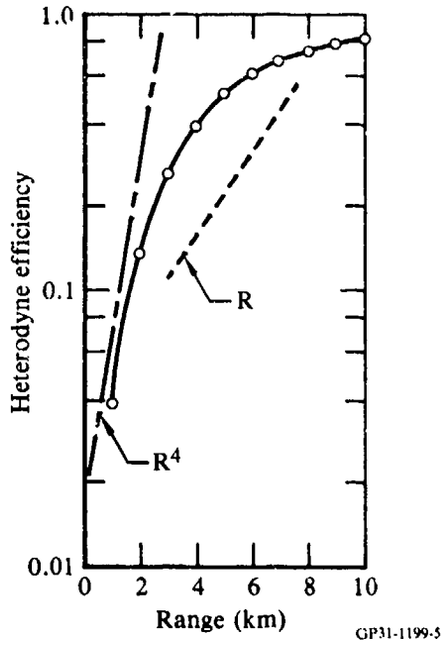

Figure 11. Calculated heterodyne-detection efficiency as a function of range for a Schell-model target with a 1-m amplitude radius. Straight lines indicate the slopes of efficiencies proportional to R and R^4 as indicated. The fixed parameters of the calculation are A = P = 2.5 cm, $f_Q = f_r = 25$ cm, $L_0 = 5$ cm, $\lambda = 10.6$ μm, and $C_n^2 = 10^{-14}$ $m^{-2/3}$.

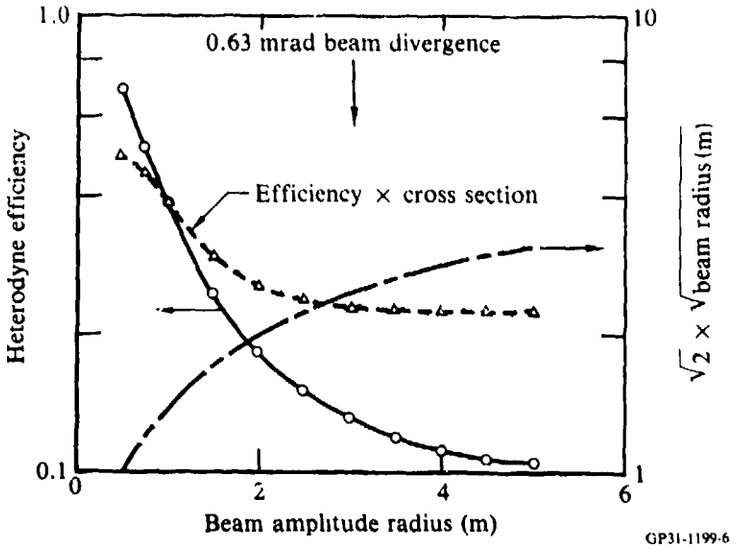

Figure 12. Calculated heterodyne-detection efficiency as a function of the amplitude beam radius for a Schell-model target. The fixed parameters of the calculation are $A = P = 2.5$ cm, $f_Q = f_r = 25$ cm, $L_0 = 5$ cm, $\lambda = 10.6$ μm, $C_n^2 = 10^{-14}$ $m^{-2/3}$, and $R = 4$ km. The laser-radar cross section is proportional to the integrated intensity distribution, which is proportional to the square root of the beam radius, which is also plotted. The relative magnitude of the product of the heterodyne efficiency and laser-radar cross section is also illustrated.

beam. The amplitude radius assumed for the range-dependent heterodyne-efficiency calculation shown in Figure 11 was 1 m. Note that although the magnitude of the efficiency values shown in Figure 11 differ from Figure 9 (as one would expect), the functional dependence is not radically different, and similar conclusions may be inferred regarding the necessity of focusing optics and the ultimate effects of atmospheric turbulence with increasing range. Similarly, the effects of beam radius shown in Figure 12 demonstrate that the actual signal-to-noise ratio does not decrease beyond a given beam radius for the Schell-model target, although a somewhat larger beam divergence is indicated for this transition. It is worth noting that there is a peak in the actual signal-to-noise ratio, although it is not illustrated in Figures 10 and 12, because the signal, perforce, goes to zero for zero beam radius.

Test Panel Calculations

A test panel configuration was devised as a simple target that could be used to validate the results of the analyses of this study in future experimental tests. Figure 13 depicts the suggested panel configuration

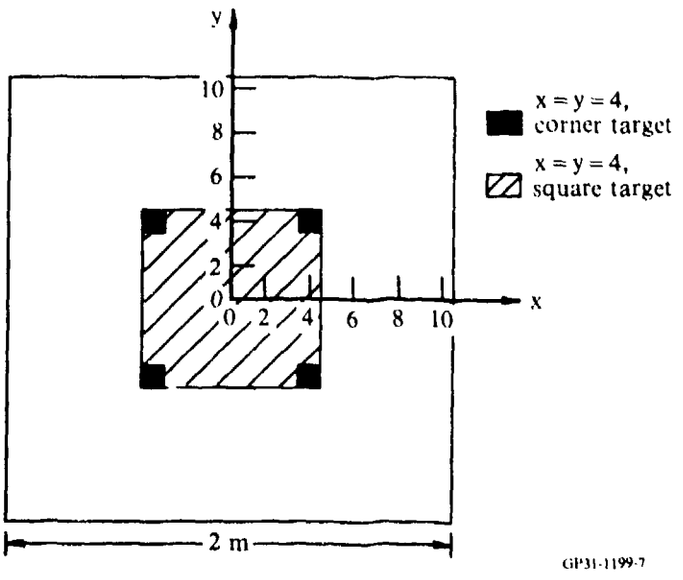

Figure 13. Depiction of suggested test-panel configuration consisting of either four 10 cm × 10 cm squares located at the corners of a square with dimensions up to 2 m × 2 m, or a square of dimensions up to 2 m × 2 m. The panel material is assumed to have a laser-radar cross section per unit area of 10^{-2}.

consisting of either small square panels, located at the corners of a large square, or a large square target of equivalent dimensions. Figure 14 shows the results of heterodyne-efficiency calculations performed as a function of the target dimensions assuming the transceiver parameters employed for the previous calculations. The Figure 14 data provide an interesting comparison between the extended target case that has previously been analyzed, and the separated target case (having a constant laser-radar cross section for various separations) that obviously gives rise to a lobing structure in the predicted heterodyne efficiency as a function of panel separation.

Several conclusions can be inferred from the separated-target heterodyne-efficiency curve shown in Figure 14. First, because the calculated negative heterodyne efficiencies, plotted as positive values in Figure 14, follow a continuous curve with the calculated positive values, it is reasonable to assume that they are, indeed, meaningful efficiency values. Thus, the physical interpretation of negative efficiency values (discussed in Section 5) as representing a quadrature component is validated to the degree that no other physical interpretation seems reasonable.

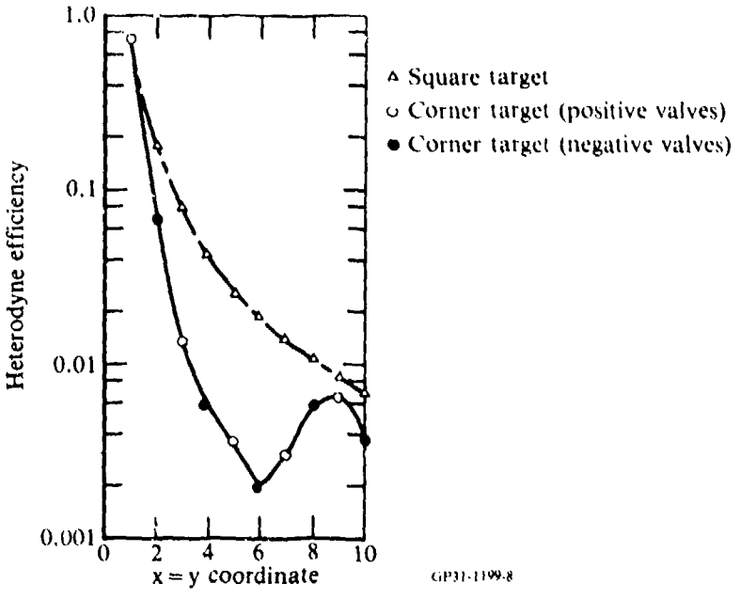

Figure 14. Calculated heterodyne-detection efficiency as a function of target extent for the two test-panel configurations shown in Fig. 13. The fixed parameters of the calculation are A = P = 2.5 cm. $f_Q = f_r = 25$ cm, $L_0 = 5$ cm, $\lambda = 10.6$ μm, $C_n^2 = 10^{-14}$ $m^{-2/3}$, and R = 1 km. The data plotted as (●) are calculated values of the heterodyne efficiency which are negative, but have been plotted as positive quantities.

Second, the lobing pattern, observed in Figure 14, is redolent of a fringe visibility pattern, such as one might obtain in a coherence experiment. Indeed, coherence effects are responsible for the degradation in heterodyne efficiency and, because of the correspondence of speckle effects with limited spatial coherence[8], it is not surprising that separated objects should give rise to a fringe-like visibility pattern at the focal plane that varies with target separation in an analogous fashion to the fringe visibility technique used to measure stellar diameters[10]. This correspondence can be demonstrated by considering the inverse problem of measuring the receiver aperture (now interpreted as an incoherent disk source) by measuring the fringe visibility at the target plane. The first null in Figure 14 is observed for a panel separation of 1.2 m, which would imply a disk size [10] of approximately 1.1 cm for the inverse problem if the fringes were obtained from two point sources. The fact that the panels are finite and arranged in a square fashion, coupled with other optical factors, accounts for disagreement between the prediction and the actual aperture diameter of 5 cm. Calculations of the heterodyne efficiency for two small panels (analogous to the pinholes

in a Young interference experiment) yields a null for a separation of 0.25 m, which corresponds to an aperture diameter of 5.2 cm for the inverse problem, which is in good agreement with the actual aperture diameter.

Finally, it is noteworthy that the lobing pattern shown in Figure 14 would be replicated in the measured signal-to-noise ratio of a laser-radar system, as well as the heterodyne efficiency, because the laser-radar cross section of the target does not vary with separation. Thus, the suggested test panel configuration provides a relatively simple means of testing some of the key predictions of the analysis, namely (a) coherence effects and (b) quadrature components.

7. GENERALIZED LASER-RADAR HETERODYNE-EFFICIENCY COMPUTER CODE

The computer code LADAR that calculates the laser-radar heterodyne efficiency for either a Schell-model target or general target cross-section distributions (assuming either a circular aperture or Cassegrain receiver geometry) is listed below. The code listing is preceded by a brief exposition of the input parameters required for its operation. All input parameters are in SI units. The code assumes a laser wavelength of 10.6 μm, which corresponds to the peak in the gain curve of the P branch [P (20)] of the $(00^{o}1) - (10^{o}0)$ band of the CO_2 laser. Alternative laser transitions can be studied using the LADAR code by editing the value assumed for the variable LAMBDA in an appropriate manner.

LADAR Input Parameters

A	- Local-oscillator aperture radius.
PIN	- Entrance-pupil inner radius. A non-zero value indicates Cassegrain geometry.
POUT	- Entrance-pupil outer radius.
FR	- Receiving lens focal length.
FL	- Local-oscillator lens focal length.
LO	- Local-oscillator Gaussian amplitude radius.
R	- Range to target.
CN2	- C_n^2 $(m^{-2/3})$
SIGPHI	- Phase variance σ_ϕ.
RADG	- Glint-point Gaussian radius of curvature.
LA	- Source amplitude radius L_A. A non-zero value indicates a Schell-model approximation.
LPHI	- Average phase-front radius of curvature $L\phi$ for the Schell-model approximation.
RHOU	- ρ_u for the Schell-model approximation.

If LA = 0, the following are required.

N1,N2 - Number of equally spaced integration points used for the numerical integration over the two components of $\vec{\xi}^{+}$.

The following parameters describe the target laser scattering distribution.

ZP1S, ZP2S - Lower bounds of the scattering distribution for the two Cartesian components of $\vec{\zeta}'$.

ZP1E,ZP2E - Upper bounds of the scattering distribution for the two Cartesian components of $\vec{\zeta}'$.

NP1,NP2 - Number of equally spaced integration points used for the numerical integration over the two components of $\vec{\zeta}'$.

D2S - NP1 x NP2 matrix of scattering distribution values. D2S (IP1,IP2) is the value of $\frac{d^2\sigma(\vec{\zeta})}{d\vec{\zeta}'^2}$ at

$$\vec{\zeta}' = \left(ZP1S + \frac{(2*IP1 - 1)}{2} \frac{(ZP1E - ZP1S)}{NP1}, \right.$$

$$\left. ZP2S + \frac{(2*IP2 - 1)}{2} \frac{(ZP2E - ZP2S)}{NP2} \right)$$

```
$FTXED
      REAL LAMBDA,K,LO,LA,LPHI
      COMMON /WAVE/ K
      COMMON /REC/ A,PIN,POUT,FR,FL,LO
      COMMON /TAR/ R,CN2,LA,LPHI,RHOU
      COMMON /CROSS/ NP1,ZP1S,ZP1E,NP2,ZP2S,ZP2E,D2S(21,21)
      DATA PI /3.141592654/
      LAMBDA=10.6E-6
      K=2.*PI/LAMBDA
      WRITE(6,1)
 1    FORMAT(' ENTER RECEIVER PARAMETERS: A,PIN,POUT,FR,FL,LO')
      READ(5,) A,PIN,POUT,FR,FL,LO
      WRITE(6,2)
 2    FORMAT(' ENTER TARGET PARAMETERS; R,CN2,SIGPHI,RADG')
      READ(5,) R,CN2,SIGPHI,RADG
      WRITE(6,6)
 6    FORMAT(' ENTER TARGET PARAMETERS; LA,LPHI,RHOU')
      LA=0.0
      READ(5,) LA,LPHI,RHOU
C CALCULATE THE COHERENT EFFICIENCY.
      CALL ECOH(EFFC)
      IF(LA.EQ.0.0) WRITE(6,11) EFFC
 11   FORMAT(' COHERENT EFFICIENCY =',G12.4)
      IF(LA.NE.0.0) WRITE(6,15) EFFC
      IF(LA.NE.0.0) STOP
      AP=A*FR/FL
      RMIN=AMIN(AP,PIN)
      RMOUT=AMIN(AP,POUT)
      WRITE(6,12) RMIN,RMOUT
 12   FORMAT(' RMIN =',G12.4,/,' RMOUT =',G12.4)
C READ INTEGRATION PARAMETERS.
      WRITE(6,3)
 3    FORMAT(' ENTER Z INTEGRATION PARAMETERS; N1,N2')
      READ(5,) N1,N2
C READ SCATTERING DISTRIBUTION.
      WRITE(6,4)
 4    FORMAT(' ENTER Z'' INTEGRATION PARAMETERS: ZP1S,ZP1E,NP1',
     1 /,34X,'ZP2S,ZP2E,NP2')
      READ(2,) ZP1S,ZP1E,NP1
      DZP1=(ZP1E-ZP1S)/NP1
      READ(2,) ZP2S,ZP2E,NP2
      DZP2=(ZP2E-ZP2S)/NP2
      WRITE(6,5)
 5    FORMAT(' ENTER SCATTERING DISTRIBUTION; D2S')
      DO 60 IP2=1,NP2
      READ(2,) (D2S(IP1,IP2),IP1=1,NP1)
 60   CONTINUE
C INTEGRATE THE SCATTERING DISTRIBUTION.
      SIGTAR=0.0
      ZP1=ZP1S+DZP1/2.
      DO 200 IP1=1,NP1
      ZP2=ZP2S+DZP2/2.
      DO 150 IP2=1,NP2
      SIGTAR=SIGTAR+D2S(IP1,IP2)
 150  ZP2=ZP2+DZP2
 200  ZP1=ZP1+DZP1
      SIGTAR=SIGTAR*DZP1*DZP2
      WRITE(6,13) SIGTAR
 13   FORMAT(' TOTAL TARGET INCOHERENT LRCS =',G12.4)
C CALCULATE THE INCOHERENT EFFICIENCY.
```

```
      CALL EINCOH(N1,N2,EFFI)
      EFFI=EFFI/SIGTAR
      WRITE(6,14) EFFI
 14   FORMAT(' INCOHERENT EFFICIENCY =',G12.4)
      TERM1=(XEXP(SIGPHI*SIGPHI)-1.)*SIGTAR
      TERM2=PI*RADH*RADG
      EPS=0.0
      IF(TERM2.NE.0.0) EPS=EPS+EFFC/(1.+TERM1/TERM2)
      IF(TERM1.NE.0.0) EPS=EPS+EFFI/(1.+TERM2/TERM1)
      IF(EPS.NE.0.0) WRITE(6,15) EPS
 15   FORMAT(' MAXIMUM HETERODYNE EFFICIENCY =',G12.4)
      STOP
      END
C -------------------------------------------------
      SUBROUTINE ECOH(EFFC)
      REAL QC(3)
      REAL LP,K,LO,LA,LPHI
      REAL LAP,LPHIP
      COMMON /WAVE/ K
      COMMON /REC/ A,PIN,POUT,FR,FL,LO
      COMMON /TAR/ R,CN2,LA,LPHI,RHOU
      COMPLEX ALPHA,BETA
      COMPLEX XCEXP
      COMMON /FINT/ ALPHA,RHOP,RM
      COMPLEX IC
      EXTERNAL F
      DATA PI,IC /3.14159265,(0.,1.)/
      RHO0=1.E6
      IF(CN2.NE.0.0) RHO0=(3.*1.455*K*K*R*CN2/8.)**(-.6)
      RHOP=RHO0
C CHECK FOR SCHELL-MODEL CALCULATION.
      IF(LA.EQ.0.0) GO TO 10
      ALPHA=CMPLX(2./K/LA,1./LPHI)
      ALPHAI=AIMAG(ALPHA)
      Z2=2.*(2.*R/K/LA)**2
      RHOP=SQRT((Z2*(RHO0**(-2)+RHOU**(-2))+CABS(1.+IC*ALPHA*R)**2)/
     1 (RHO0**(-2)*(1.-2.*K*ALPHAI+CABS(ALPHA*R)**2)+
     2 RHO0**(-2)*(R*ALPHAI+.75*Z2*RHO0**(-2))+
     3 RHOU**(-2)*(1.+RHO0**(-2)*Z2)))
      LAP=LA*SQRT(Z2*(RHO0**(-2)+RHOU**(-2))+CABS(1.+IC*ALPHA*R)**2)
      LPHIP=R*(Z2*(RHO0**(-2)+RHOU**(-2))+CABS(1.+IC*ALPHA*R)**2)/
     1 (ALPHAI*R-CABS(ALPHA*R)**2-Z2*(.5*RHO0**(-2)+RHOU**(-2)))
 10   CONTINUE
      AP=A*FR/FL
      Z=K/2.*(1./FL-1./FR)
      ZP=Z*(FR/K)**2
      LP=LO*FR/FL
      BETA=CMPLX(LP*LP,-4.*ZP)/(LP**4+16.*ZP**2)
      IF(LA.EQ.0.0) ALPHA=BETA+CMPLX(RHOP**(-2),K/2./R)
      IF(LA.NE.0.0) ALPHA=BETA+CMPLX(RHOP**(-2)+1./LAP,K/2./LPHIP)
      BETAR=REAL(BETA)
      RMIN=AMIN(AP,PIN)
      RMOUT=AMIN(AP,POUT)
      DO 100 I=1,3
      QC(I)=0.
      RM1=RMIN
      RM2=RMOUT
C CHECK FOR CASSEGRAIN RECEIVER GEOMETRY.
      IF(RMIN.EQ.0.0 .AND. I.GT.1) GO TO 100
      IF(I.EQ.1) RM1=RMOUT
```

```
      IF(I.EQ.3) RM2=RMIN
C CALCULATE THE COHERENT INTEGRAL.
      XCE1=1.-XCEXP(-ALPHA*RM1*RM1)-XCEXP(-CONJG(ALPHA)*RM2*RM2)
      XCE2=XCEXP(-ALPHA*RM1*RM1-CONJG(ALPHA)*RM2*RM2+
     1 2.*RM1*RM2/RHOP/RHOP)
      QC(I)=(XCE1+XCE2*EIC(2.*RM1*RM2/RHOP/RHOP))/4./CABS(ALPHA)**2
      RM=RM2
      CALL SIMP(F,0.,RM1,0.01,10,SP,SF,NI,IER)
      IF(RM1.EQ.RM2) SF=2.0*SF
      QC(I)=QC(I)-RM2*SF/2./(CABS(ALPHA)*RHOP)**2
      IF(RM1.EQ.RM2) GO TO 50
      RM=RM1
      CALL SIMP(F,0.,RM2,0.01,10,SP,SF,NI,IER)
      QC(I)=QC(I)-RM1*SF/2./(CABS(ALPHA)*RHOP)**2
 50   QC(I)=QC(I)*4./(1.0-1.0/(CABS(ALPHA)*RHOP*RHOP)**2)
 100  CONTINUE
      EFFC=2.*BETAR/(ROUT**2-RIN**2)*(QC(1)-2.*QC(2)+QC(3))/
     1 (XEXP(-2.*BETAR*RMIN**2)-XEXP(-2.*BETAR*RMOUT**2))
      RETURN
      END
C -------------------------------------------------
      SUBROUTINE EINCOH(N1,N2,EFFI)
      REAL QI(3)
      REAL LP,K,LO,LA,LPHI
      COMMON /WAVE/ K
      COMMON /REC/ A,PIN,POUT,FR,FL,LO
      COMMON /TAR/ R,CN2,LA,LPHI,RHOO
      COMMON /CROSS/ NP1,ZP1S,ZP1E,NP2,ZP2S,ZP2E,D2S(21,21)
      COMPLEX ALPHA,BETA
      REAL JINC
      COMPLEX IC
      DATA PI,IC /3.14159265,(0.,1.)/
      RHOO=1.E6
      IF(CN2.NE.0.0) RHOO=(3.*1.455*K*K*R*CN2/8.)**(-.6)
      RHOP=RHOO
      AP=A*FR/FL
      Z=K/2.*(1./FL-1./FR)
      ZP=Z*(FR/K)**2
      LO=LO*FR/FL
      BETA=CMPLX(LP*LP,-4.*ZP)/(LP**4+16.*ZP**2)
      ALPHA=BETA+CMPLX(RHOP**(-2),K/2./R)
      BETAR=REAL(BETA)
      BETAI=AIMAG(BETA)
      BETAI=BETAR+2./RHOP/RHOP
      RMIN=AMIN(AP,PIN)
      RMOUT=AMIN(AP,POUT)
      CONST=2.*R/K*BETAI+1.0
      DO 500 I=1,3
      QI(I)=0.
      RP=RMOUT
C CHECK FOR CASSEGRAIN RECEIVER GEOMETRY.
      IF(RMIN.EQ.0.0 .AND. I.GT.1) GO TO 500
      IF(I.EQ.2) RP=(RMIN+RMOUT)/2.
      IF(I.EQ.3) RP=RMIN
      RM=RP
      IF(I.EQ.2) RM=SQRT((RMIN**2+RMOUT**2)/2.)
C CALCULATE THE INCOHERENT INTEGRAL.
      D71=2.*RP/N1
      Z1S=-RP
      D72=2.*RP/N2
```

```
      Z2S=-RP
      DZP1=(ZP1E-ZP1S)/NP1
      DZP2=(ZP2E-ZP2S)/NP2
      EPS=0.0
      Z1=Z1S+DZ1/2.
      DO 400 I1=1,N1
      Z2=Z2S+DZ2/2.
      DO 300 I2=1,N2
      IF(Z1*Z1+Z2*Z2.GT.RP*RP) GO TO 300
      ZP1=ZP1S+DZP1/2.
      DO 200 IP1=1,NP1
      ZP2=ZP2S+DZP2/2.
      DO 100 IP2=1,NP2
      IF(D2S(IP1,IP2).EQ.0.0) GO TO 100
      UP=SQRT((Z1*CONST+ZP1)**2+(Z2*CONST+ZP2)**2)*K/R
      A=2.*SQRT(RM*RM-Z1*Z1-Z2*Z2)
      IF(UP.LT.BETAT*A) GO TO 80
      FT=2.*PI*A*A*JINC(UP*A)
      GO TO 90
   80 FT=2.*PI*(XEXP(-UP*UP/2./BETAT)/BETAT-XEXP(-A*A/2.*(
     1 BETAT+UP*UP/2.))/(BETAT+UP*UP/2.))
   90 CONTINUE
      EPS=EPS+XEXP(-2.*BETAR*(Z1*Z1+Z2*Z2))*FT*D2S(IP1,IP2)
  100 ZP2=ZP2+DZP2
  200 ZP1=ZP1+DZP1
  300 Z2=Z2+DZ2
  400 Z1=Z1+DZ1
      QI(I)=EPS*DZ1*DZ2*DZP1*DZP2
  500 CONTINUE
      EFFI=BETAR/PI/PI/(POUT**2-PIN**2)*(QI(1)-2.*QI(2)+QI(3))/
     1 (XEXP(-2.*BETAR*RMIN**2)-XEXP(-2.*BETAR*RMOUT**2))
      RETURN
      END
C -------------------------------------------------
      FUNCTION F(Y)
      COMPLEX ALPHA,XCEXP
      COMMON /FINT/ ALPHA,RC,RM
      F=XCEXP(-ALPHA*Y*Y-CONJG(ALPHA)*RM*RM+2.*Y*RM/RC/RC)
      IF(F.EQ.0.0) RETURN
      F=F*EI1(2.*Y*RM/RC/RC)
      RETURN
      END
C -------------------------------------------------
      COMPLEX FUNCTION XCEXP(W)
      COMPLEX W
      XCEXP=(0.,0.)
      IF(REAL(W).LT.-650.) RETURN
      XCEXP=CEXP(W)
      RETURN
      END
C -------------------------------------------------
      FUNCTION XEXP(X)
      XEXP=0.0
      IF(X.LT.-650.) RETURN
      XEXP=EXP(X)
      RETURN
      END
C -------------------------------------------------
      REAL FUNCTION JINC(X)
      IF(X.GT.3.0) GO TO 100
```

```
      T=(X/3.0)**2
      JINC=0.5+T*(-0.56249985+T*(0.21093573+T*(-0.03954289+
     1 T*(0.00443319+T*(-0.00031761+T*0.00001109)))))
      RETURN
  100  T=3.0/X
      F1=0.79788456+T*(0.00000156+T*(0.01659667+T*(0.00017105+
     1 T*(-0.00249511+T*(0.00113653-T*0.00020033)))))
      THETA1=X-2.35619449+T*(0.12499612+T*(0.00005650+T*(
     1 -0.00637879+T*(0.00074348+T*(0.00079824-T*0.00029166)))))
      JINC=F1*COS(THETA1)/X**(1.5)
      RETURN
      END
C -------------------------------------------------------
      FUNCTION EI0(X)
C COMPUTE EXP(-X) * I0.
      IF(X.GT.3.75) GO TO 100
      T=(X/3.75)**2
      EI0=1.+T*(3.5156229+T*(3.0899424+T*(1.2067492+T*(
     1 .2659732+T*(.0360768+T*.0045813)))))
      EI0=EXP(-X)*EI0
      RETURN
  100  T=3.75/X
      EI0=.39894228+T*(.01328592+T*(.00225319+T*(-.00157565+
     1 T*(.00916281+T*(-.02057706+T*(.02635537+T*(-.01647633+
     2 T*.00392377)))))))
      EI0=EI0/SQRT(X)
      RETURN
      END
C -------------------------------------------------------
      FUNCTION EI1(X)
C COMPUTE EXP(-X) * I1.
      IF(X.GT.3.75) GO TO 100
      T=(X/3.75)**2
      EI1=0.5+T*(.87890594+T*(.51498869+T*(.15084934+T*(
     1 .02658733+T*(.00301532+T*.00032411)))))
      EI1=EI1*X
      EI1=EXP(-X)*EI1
      RETURN
  100  T=3.75/X
      EI1=.39894228+T*(-.03988024+T*(-.00362018+T*(.00163801+
     1 T*(-.01031555+T*(.02282967+T*(-.02895312+T*(
     2 .01787654+T*(-.00420059)))))))
      EI1=EI1/SQRT(X)
      RETURN
      END
C -------------------------------------------------------
      SUBROUTINE SIMP(F,A,B,DEL,IMAX,SI1,S,N,IER)
C SIMPSON INTEGRATION ROUTINE.
      N=0
      BA=B-A
      IF (BA)20,19,20
   19 IER=1
      RETURN
   20 IF(DEL)22,22,23
   22 IER=2
      RETURN
   23 IF(IMAX-1)24,24,25
   24 IER=3
      RETURN
   25 X=BA/2.+A
```

```
      NHALF=1
      SUMK=F(X)*BA*2./3.
      S=SUMK+(F(A)+F(B))*BA/6.
      DO 28 I=2,IMAX
      SI1=S
      S=(S-SUMK/2.)/2.
      NHALF=NHALF*2
      ANHLF=NHALF
      FRSTX=A+(BA/ANHLF)/2.
      SUMK=F(FRSTX)
      XK=FRSTX
      KLAST=NHALF-1
      FINC=BA/ANHLF
      DO 26 K=1,KLAST
      XK=XK+FINC
   26 SUMK=SUMK+F(XK)
      SUMK=SUMK*2.*BA/(3.*ANHLF)
      S=S+SUMK
      IF(S.EQ.0.0) GO TO 29
      IF((ABS(S-SI1)/ABS(S))-DEL) 29,28,28
   28 CONTINUE
      IER=4
      GO TO 30
   29 IER=0
   30 N=2*NHALF
      RETURN
      END
```

REFERENCES

1. J. C. Leader, "Laser Radar Analyses," McDonnell Douglas Report MDC Q0714, 15 July 1980, Final Report on Naval Surface Weapons Center Contract No. N60921-79-C-0180.
2. J. C. Leader, "Bandpass Filtering of Moving-Object Laser Heterodyne Signals by Finite Apertures," Appl. Opt. 17, 1194 (1978).
3. J. C. Leader, "Beam Properties of Partially Coherent Curved Beam Waves in the Turbulent Atmosphere," J. Opt. Soc. Am. 70, 682 (1980).
4. J. C. Leader, "Atmospheric Propagation of Partially Coherent Radiation," J. Opt. Soc. Am. 68, 195 (1978).
5. J. C. Leader, "Detection Efficiency for Large-Aperture Coherent Laser Radars," SPIE Proc. on Physics and Technology of Coherent Infrared Radar, 300, 74 (1981).
6. S. F. Clifford and S. Wandzura, "Monostatic Heterodyne LIDAR Performance: The Effect of the Turbulent Atmosphere," Appl. Opt. 20, 514 (1981).
7. S. H. Shapiro, B. A. Capron, and R. C. Harney, "Imaging and Target Detection with a Heterodyne-Reception Optical Radar," Appl. Opt. 20, 3292 (1981).
8. J. C. Leader, "Similarities and Distinctions Between Coherence Theory Relations and Laser Scattering Phenomena," Opt. Eng. 19, 593 (1980).
9. G. P. Jacobs, "Heterodyne Laser Efficiency Measurements," General Electric Co., Electronics Laboratory Final Report on Contract N60921-80-C-0085.
10. M. J. Brown and G. B. Parrent, Theory of Partial Coherence, (Prentice-Hall, Englewood, NJ, 1964).
11. S. F. Clifford, NOAA, Boulder, CO., private communication.
12. J. C. Leader, "Analysis and Prediction of Laser Scattering from Rough Surface Materials," J. Opt. Soc. Am. 69, 610 (1979).

BIBLIOGRAPHY

Antenna Gain and Heterodyne Detection

1. L. G. Kazovsky and N. S. Kopeika, "Heterodyne Detection Through Rain, Snow, and Turbid Media: Effective Receiver Size at Optical Through Millimeter Wavelengths," Appl. Opt. 22, 70 No.5 (1983).
2. B. J. Klein and J. J. Degnan, "Optical Antenna Gain. 1: Transmitting Antennas," Appl. Opt. 13, No. 9, 2134 (1974).
3. B. J. Rye, "Primary Aberration Contribution to Incoherent Backscatter Heterodyne LIDAR Returns," Appl. Opt. 21, No. 5, 839 (1982).
4. N. Saga, K. Tanaka, and O. Fukumitsu, "Diffraction of a Gaussian Beam Through a Finite Aperture Lens and the Resulting Heterodyne Efficiency," Appl. Opt. 20, No. 16, 2827 (1981).
5. J. Salzman and A. Katzir, "Signal-to-Noise Ratio of Heterodyne Detection: Matrix Formalism," Appl. Opt. 22, No. 6, 888 (1983).
6. A. E. Siegman, "The Antenna Properties of Optical Heterodyne Receivers," Proc. IEEE 56, No. 10, 1350 (1966).

Atmospheric Effects Pertinent to Laser Radar

7. L. R. Bissonnette, "Propagation Model of Laser Beams in Turbulence," J. Opt. Soc. Am. 73, No. 3, 262 (1983).
8. P. Bruscaglioni, G. Milloni, and G. Zaccanti, "On the Contribution of Multiple Scattering to LIDAR Returns from Homogeneous Fogs and Its Dependence on the LIDAR Range and on the Receiver Angular Aperture," Optica Acta 27, No. 8, 1229 (1980).
9. A. I. Carswell and S. R. Pal, "Polarization Anisotropy in LIDAR Multiple Scattering From Clouds," Appl. Opt. 19, No. 24, 4123 (1980).
10. A. Deepak and M. A. Box, "Forwardscattering Corrections for Optical Extinction Measurements in Aerosol Media. 1: Monodispersions," Appl. Opt. 17, No. 18, 2900 (1978).
11. D. A. de Wolf, "Coherence of a Light Beam Through an Optically Dense Turbid Layer," Appl. Opt. 17, No. 8, 1280 (1978).

12. J. C. Leader, "Atmospheric Propagation of Partially Coherent Radiation," J. Opt. Soc. Am. 68, 175 (1978).
13. J. C. Leader, "Beam Intensity Fluctuations in Atmospheric Turbulence," J. Opt. Soc. Am. 71, 542, (1981).
14. J. C. Leader, "Beam Properties of Partially Coherent Curved Beam Waves in the Turbulent Atmosphere," J. Opt. Soc. Am. 70, No. 6, 682 (1980).
15. J. C. Leader, "Far-Zone Range Criteria for Quasi-Homogeneous Partially Coherent Sources," J. Opt. So. Am. 68, 1332 (1978).
16. J. C. Leader, "Intensity Fluctuations Resulting from the Propagation of Partially Coherent Beam Waves in the Turbulent Atmosphere," SPIE 23rd Annual Technical Symposium, San Diego, CA, 27-30 Aug 1979, MDRL Report No. 79-32.
17. J. C. Matter and R. G. Bradley, "Optical Pulse Propagation Through Clouds," Appl. Opt. 20, No. 4, 554, (1981).
18. G. C. Mooradian, M. Geller, L. B. Stotts, D. H. Stephens, and R. A. Krautwald, "Blue-Green Pulsed Propagation through Fog," Appl. Opt. 18, No. 4, 429 (1979).
19. W. S. Ross, W. P. Jaeger, J. Nakai, T. T. Nguyen, and J. H. Shapiro, "Atmospheric Optical Propagation - An Integrated Approach," Opt. Eng. 21, No. 4, 775, (1982).
20. J. S. Ryan, M. H. Hubert, and R. A. Crane, "Water Vapor Absorption at Isotopic CO_2 Laser Wavelengths," Appl. Opt. 22, No. 5, 711 (1983).
21. L. Stefanuti and L. Pantani, "LIDAR Visibility Measurements in Italy", Optica Acta 27, No. 8, 1243 (1980).
22. G. W. Sutton and D. H. Douglas-Hamilton, "CO_2 (10.6 μm) Atmospheric Propagation Enhancement Due to Off-Line Center Tuning," Appl. Opt. 18, No. 13, 2323 (1979).
23. W. G. Tam and A. Zardecki, Off-axis Propagation of a Laser Beam in Low Visibility Weather Conditions," Appl. Opt. 19, No. 16, 2822 (1980).
24. L. S. Taylor, "Infrared Noise Caused by Turbulent Flows," Appl. Opt. 17, No. 24, 3911 (1978).

Laser Heterodyne Detection

25. F. E. Goodwin and M. E. Pedinoff, "Application of CCl_4 and CCl_2:CCl_2 Ultrasonic Modulators to Infrared Optical Heterodyne Experiments," Appl. Phys. Lett. 8, No. 3, 60 (1966).

26. G. Gould, S. F. Jacobs, J. T. LaTourrette, M. Newstein, and P. Rabinowitz, "Coherent Detection of Light Scattered from a Diffusely Reflecting Surface," Appl. Opt. 3, No. 5, 648 (1964).

27. N. H. Farhat, D. G. Herzog, R. J. Tarazaiski, and H. M. Weiskittel, "Target-Synthesized Optical Apertures," J. Opt. Soc. Am. 63, No. 11, 1403 (1973).

28. D. Fink and S. N. Vodopia, "Coherent Detection SNR of an Array of Detectors," Appl. Opt. 15, No. 2, 453 (1976).

29. D. L. Fried, "Equivalence of Near-Field and Far-Field Heterodyne Measurements of Diffuse Target Cross-Section," Optical Science Consultants Report No. TR-242 (1977).

30. J. Hanlon and S. F. Jacobs, "Narrowband Optical Heterodyne Detection," IEEE J. Quantum Electron., p. 242 (1967 IEEE Conf. on Laser Engineering & Applications).

31. C. W. Helstrom, "Detectability of Coherent Optical Signals in a Heterodyne Receiver," J. Opt. Soc. Am. 57, No. 3, 353 (1967).

32. J. Leblond and El S. El Badawy, "Laser Doppler Velocimetry Using a Superheterodyne Spectrum Analyzer," Appl. Opt. 14, No. 4, 902 (1975).

33. L. Mandel, "Heterodyne Detection of a Weak Light Beam," J. Opt. Soc. Am. 56, No. 9, 1200 (1966).

34. J. H. Shapiro, "Signal Processing for a Signal with Poisson Noise: Comments," Appl. Opt. 13, No. 11, 2462 (1974).

35. A. E. Siegman, "A Maximum-Signal Theorem for the Spatially Coherent Detection of Scattered Radiation," IEEE Trans. Antennas Propagat., p. 192 (1967).

36. M. C. Teich, "Infrared Heterodyne Detection," Proc. IEEE 56, No. 1, 37 (1968).

37. M. C. Teich and R. Y. Yen, "Three-Frequency Nonlinear Heterodyne Detection. 1: cw Radar and Analog Communications," Appl. Opt. 14, No. 3, 666 (1975).

38. M. C. Teich and R. Y. Yen, "Three-Frequency Nonlinear Heterodyne Detection. 2: Digital Communications and Pulsed Radar," Appl. Opt. 14, No. 3, 680 (1975).

Laser Radar Measurements

39. R. M. Hardesty, R. J. Keeler, M. J. Post, and R. A. Frichter, "Characteristics of Coherent LIDAR Returns from Calibration Targets and Aerosols," Appl. Opt. 20, No. 21, 3763 (1981).
40. G. B. Jacobs, "Heterodyne Laser Efficiency Measurements," Final Report for NSWC Contract No. N60921-80-C-0085 (1982).
41. D. K. Killinger, N. Menyuk, and W. E. DeFeo, "Experimental Comparison of Heterodyne and Direct Detection for Pulsed Differential Absorption CO_2 LIDAR," Appl. Opt. 22, No. 5, 682 (1983).
42. N. Menyuk and D. K. Killinger, "Temporal Correlation Measurements of Pulsed Dual CO_2 LIDAR Returns," J. Opt. Lett. 6, No. 6, 301 (1981).
43. R. L. Schwiesow and R. F. Calfee, "Atmospheric Refractive Effects on Coherent LIDAR Performance at 10.6 μm," Appl. Opt. 18, No. 23, 3911 (1979).

Laser Radar Technology

44. F. R. Arams, E. W. Sard, B. J. Peyton, and F. P. Pace, "5.2-Infrared 10.6-Micron Heterodyne Detection with Gigahertz IF Capability," IEEE J. Quantum Electron. QE-3, No. 11, 484 (1967).
45. J. M. Cruickshank, "Transversely Excited Atmospheric CO_2 Laser Radar with Heterodyne Detection," Appl. Opt. 18, No. 3, 290, (1979).
46. A. V. Jelalian, "Laser and Microwave Radar," Laser Focus, 88 (1981).
47. U. P. Oppenheim and R. T. Menzies, "Aligning the Transmitter and Receiver Telescopes of an Infrared LIDAR: A Novel Method," Appl. Opt. 21, No. 2, 174 (1982).
48. R. L. Schwiesow and L. Lading, "Temperature Profiling by Rayleigh-Scattering LIDAR," Appl. Opt. 20, No. 11, 1972 (1981).
49. W. B. Veldkamp, "Holographic Local-Oscillator Beam Multiplexing for Array Heterodyne Detection," Appl. Opt. 22, No. 6, 891 (1983).
50. W. B. Veldkamp and C. J. Kastner, "Beam Profile Shaping for Laser Radar that Use Detector Arrays," Appl. Opt. 21, No. 2, 345 (1982).

Target Reflectivity

51. J. W. Goodman, "Some Effects of Target-Induced Scintillation on Optical Radar Performance," Proc. IEEE 53, No. 11, 1688 (1965).
52. J. C. Leader, "Analysis and Prediction of Laser Scattering from Rough-Surface Materials", J. Opt. Soc. Am. 69, 610 (1979).
53. M. J. Post, R. A. Richter, R. J. Keeler, R. M. Hardesty, T. R. Lawrence, and F. F. Hall, "Calibration of Coherent LIDAR Targets", Appl. Opt. 19, No. 16, 2828 (1980).
54. J. B. Schut, B. N. Holben, C. M. Shai, and J. H. Henninger, "Reflectivity of TFE - A Washable Surface - Compared with that of $BaSO_4$," Appl. Opt. 20, No. 12, 2033 (1981).
55. J. H. Shapiro, "Target-Reflectivity Theory for Coherent Laser Radars," Appl. Opt. 21, No. 18, 3398 (1982).
56. T. W. Stuhlinger, E. L. Dereniak, and F. O. Bartell, "Bidirectional Reflectance Distribution Function of Gold-Plated Sandpaper," Appl. Opt. 20, No. 15, 2648 (1981).

Turbulent and Target Effects on Heterodyne Detection

57. J. H. Churnside and C. M. McIntyre, "Joint Signal Current Probability Distribution for Optical Heterodyne Receiver Arrays in the Turbulent Atmosphere," Appl. Opt. 18, No. 13, 2315 (1979).
58. J. H. Churnside and C. M. McIntyre, "Partial Tracking Optical Heterodyne Receiver Arrays," J. Opt. Soc. Am. 68, No. 12, 1672 (1978).
59. P. Ciolli, A. Consortini, P. Pandolfini, F. Pasqualetti, L. Ronchi, and R. Vanni, "Effect of Recording Process in Evaluating Higher-Order Propagation Statistics," J. Opt. Soc. Am. 68, No. 10, 1350 (1978).
60. S. F. Clifford and S. Wandzura, "Monostatic Heterodyne LIDAR Performance: The Effect of the Turbulent Atmosphere," Appl. Opt. 20, No. 3, 514 (1981).
61. D. L. Fried, "Optical Heterodyne Detection of an Atmospherically Distorted Signal Wave Front", Proc. IEEE 55, No. 1, 57 (1967).

62. J. C. Leader, "Detection Efficiency for Large-Aperture Coherent Laser Radars," Physics and Technology of Coherent Infrared Radar Meeting of the Society of Photo-Optical Instrumentation Engineers, San Diego, CA 24-28 Aug 1981, MDRL Report No. 81-18.

63. B. J. Rye, "Refractive-Turbulence Contribution to Incoherent Backscatter Heterodyne LIDAR Returns," J. Opt. Soc. Am. 71, No. 6, 687 (1981).

64. J. H. Shapiro, B. A. Capron, and R. C. Harney, "Imaging and Target Detection with a Heterodyne-Reception Optical Radar," Appl. Opt. 20, No. 19, 3292 (1981).

65. J. H. Shapiro and S. T. Lau, "Turbulence Effects on Coherent Laser Radar Target Statistics," Appl. Opt. 21, No. 13, 2395 (1982).

66. J. Y. Wang, "Heterodyne Laser Radar SNR from a Diffuse Target Containing Multiple Glints," Appl. Opt. 21, No. 3, 464 (1982).

67. R. E. Warren, "Multiple Pulse Detection in Atmospheric Turbulence," Appl. Opt. 17, No. 17, 2721 (1978).